Revealing magma degassing below closed-conduit active volcanoes: geochemical features of volcanic rocks versus fumarolic fluids at Vulcano (Aeolian Islands, Italy)

Michela Mandarano[1], Antonio Paonita[1], Mauro Martelli[1],
Marco Viccaro[2], Eugenio Nicotra[2,3], Ian L. Millar[4]

[1] Istituto Nazionale di Geofisica e Vulcanologia (INGV) – Sezione di Palermo, Via Ugo La Malfa 153, 90146 Palermo (Italy)
[2] Università degli studi di Catania, Dipartimento di Scienze Biologiche Geologiche e Ambientali, Corso Italia 57, 95129 Catania (Italy)
[3] Università della Calabria, Dipartimento di Biologia, Ecologia e Scienze della Terra, Via P. Bucci 15/B, 87036 Arcavacata di Rende (Italy)
[4] British Geological Survey, NERC Isotope Geosciences Labs, Kingsley Dunham Centre, Keyworth, NG12 5GG, Nottingham (England)

Corresponding author: Antonio Paonita, e-mail: antonio.paonita@ingv.it

REVISED VERSION

Abstract

The elemental and isotopic compositions of noble gases (He, Ne, and Ar) in olivine- and clinopyroxene-hosted fluid inclusions have been measured for rocks at various degrees of evolution and belonging to high-K calcalkaline–shoshonitic and shoshonitic–potassic series in order to cover the entire volcanological history of Vulcano Island (Italy). The major- and trace-element concentrations and the Sr- and Pb-isotope compositions for whole rocks were integrated with data obtained from the fluid inclusions. $^{3}He/^{4}He$ in fluid inclusions is within the range of 3.30 and 5.94 R/Ra, being lower than the theoretical value for the deep magmatic source expected for Vulcano Island (6.0–6.2 R/Ra). $^{3}He/^{4}He$ of the magmatic source is almost constant throughout the volcanic history of Vulcano. Integration of the He- and Sr-isotope systematics leads to the conclusion that a decrease in the He-isotope ratio of the rocks is mainly due to the assimilation of 10–25% of a crustal component similar to the Calabrian basement. $^{3}He/^{4}He$ shows a negative correlation with Sr isotopes except for the last-erupted Vulcanello latites (Punta del Roveto), which have anomalously high He isotope ratios. This anomaly has been attributed to a flushing process by fluids coming from the deepest reservoirs, since an input of deep magmatic volatiles with high $^{3}He/^{4}He$ values increases the He-isotope ratio without changing $^{87}Sr/^{86}Sr$. A comparison of the He-isotope ratios between fluid inclusions and fumarolic gases shows that only the basalts of La Sommata and the latites of Vulcanello have comparable values. Taking into account that the latites of Vulcanello relate to one of the most-recent eruptions at Vulcano (in the 17th century), we infer that that the most probable magma which actually feeds the fumarolic emissions is a latitic body that ponded at about 3–3.5 km of depth and is flushed by fluids coming from a deeper and basic magma.

Keywords

Helium isotopes, radiogenic isotopes, fluid inclusions, rock geochemistry, arc volcanism

1. Introduction

Volcanoes that exhibit explosive activity can also undergo periods of quiescence lasting from hundreds to thousands of years, during which the magmas can experience closed-system storage conditions. During these long-lasting phases, volcanic degassing mainly occurs via fumarolic activity at the crater bottom and/or flanks, in addition to diffuse soil degassing and hydrothermal circulation. This activity testifies to the presence of magmas that exsolve volatiles at depth and are likely to lead to future increases in the volcanic activity. Hence, an increased awareness of these degassing magma bodies is of primary importance to volcanic surveillance. The main questions to be addressed relate to the localization, composition, and volatile contents of the magma bodies that feed the volcanic degassing. All of these features can be interdependent and have a strong impact on the magnitude and type of the expected eruptive events (Parfitt and Wilson, 2008).

The volcanic system of Vulcano (Aeolian Islands, Italy) is a suitable natural laboratory for exploring this topic. The last eruptive event at Vulcano occurred during 1888–1890 AD, and since this time the volcano has been in a state of quiescence, with volcanic manifestations mainly characterized by intense exhalations and moderate seismic activity related to the migration of magmatic and hydrothermal fluids (Peccerillo et al., 2006; Cannata et al., 2011). There have been several phases of unrest since the last eruption, as testified by geochemical anomalies measured in fumarolic gases emitted at the La Fossa cone. Various authors have attributed this unrest to an increasing contribution of fluids coming from magmas at depth (Nuccio et al., 1999; Chiodini et al., 2000; Paonita et al., 2002, 2013; Taran, 2011). With the aim of understanding the types of magma involved in these deep dynamics, several geochemical and petrological studies have been carried out (Clocchiatti et al., 1994a; Magro, 1997; Nuccio et al., 1999; Paonita et al., 2002, 2013; Granieri et al., 2006). The results have suggested that the compositions of these degassing magmas can range from basaltic to intermediate, although Paonita et al. (2013) recently constrained the composition to latite.

The most intriguing goal of this work is the search for relationships between the magma that is actually degassing within the plumbing system and the fumarolic fluids. A comparison between the composition of the volatiles entrapped in erupted products and that of the fumarolic fluids has been conducted in order to achieve this. Attention has been focused on He isotopes, which are regarded to be the best tracers of magma-derived fluids and make it possible to obtain *a posteriori* information on magmatic conditions before an eruptive event (Marty et al., 1994; Hilton et al., 2002; Nuccio et al., 2008). In this regard, a large set of He isotopic data of the fumarolic fluids are already available from previous studies (Tedesco and Nagao, 1996; Capasso et al., 1997; Nuccio et al., 1999, 2001; Tedesco and Scarsi, 1999; Paonita et al., 2002, 2013; Taran, 2011). Measurements

of the elemental and isotopic compositions of He and Ar retained in fluid inclusions hosted by mafic minerals—together with the major and trace elements and the Sr- and Pb-isotope ratios for the whole rocks—have been obtained from rocks at different evolutionary degree (from basalt to trachyte), covering all of the main stages of volcanic activity at Vulcano Island. The data obtained in the present study extend and complete the data set reported by Magro (1997) and Martelli et al. (2008). The new results presented here suggest the presence of a well-structured feeding system that is characterized by small and shallow batches of latitic magmas flushed by volatiles coming from a deep magma chamber with a basaltic composition.

2. Geological and volcanological setting

2.1 Geology and petrology

Vulcano is the southernmost island of the Aeolian Islands, a Quaternary volcanic arc generated by subduction of the oceanic Ionian plate underneath the Calabrian arc (Finetti and Del Ben, 1986). The Aeolian Islands are located on 15- to 20-km-thick continental crust (Peccerillo et al., 2006) related to the Hercynian metamorphic and granitic rocks and Mesozoic sediments of the Calabrian basement (Keller, 1980; Del Moro et al., 1998; Frezzotti et al., 2004). Vulcano is part of a volcanic complex including Lipari Island that has developed inside a graben-like structure controlled by the NNW–SSE strike-slip Tindari-Letojanni fault system (Gioncada et al., 2003; Ventura, 2013).

The subaerial volcanic activity at Vulcano started at about 120–100 ka (Keller, 1980) in the southern sector of the island with the building of Primordial Vulcano stratocone. A volcano tectonic collapse occurred at 100 ka that led to the formation of the Piano Caldera (Keller, 1980), where intracaldera activity took place until 21 ka. Poorly evolved products belonging to the high-K calcalkaline (HKCA) and shoshonitic (SHO) series were emitted during these two stages of activity, whereas more-evolved rocks erupted during the emplacement of rhyolitic domes and trachytic lava flows of the Lentia Complex between 25 and 15 ka (Keller, 1980; De Astis et al., 1997, 2013). After the collapse of the Lentia domes at 15 ka, phreatomagmatic activity shifted toward the north, with the formation of several vents active along an N–S direction (Saraceno, La Fossa cone, Faraglione, and Vulcanello), with the emission of volcanic products with compositions varying from latitic to rhyolitic [SHO and potassic (KS) series], and only minor amounts of shoshonites (Keller, 1980; De Astis et al., 1997; Gioncada et al., 2003). The La Fossa cone formed at about 5.5 ka through accretion due to the deposition of pyroclastic products and minor lava flows. The Vulcanello peninsula is a 123-m-high composite edifice comprising a shoshonitic to latitic lava platform and three partially overlapping scoria cones aligned in an NE–SW direction along the

123 northern ring fault of the La Fossa caldera (Davì et al., 2009a; De Astis et al., 2013). Although the
124 age of Vulcanello products is still debated, some recent studies using archaeomagnetic
125 investigations have suggested that the lava platform was built up during continuous volcanic
126 activity from 1100 to 1250 AD (Arrighi et al., 2006; Davì et al., 2009a; Di Traglia et al., 2013 and
127 references therein). The three stratocones at Vulcanello formed between 1050±70 AD and the 17th
128 century (Fusillo et al., 2015 and references therein). The last eruption at Vulcano Island occurred
129 during 1888–1890, with the characteristic eruptive activity defined as "Vulcanian" by Mercalli and
130 Silvestri (1891).
131
132 *2.2 Geochemistry of fluids*
133 Vulcano Island is currently in a state of intense fumarole activity chiefly localized in the northern
134 rim of the La Fossa cone and in the area of Baia Levante, while CO_2 soil degassing occurs around
135 the cone (Capasso et al., 1997; Inguaggiato et al., 2012). These manifestations are characterized by
136 gas emissions with differing temperature and chemical compositions. The fluids emitted from the
137 fumarole field at the La Fossa crater are characterized by high temperatures (100–450°C) and a
138 typical magmatic origin with high concentrations of CO_2, N_2, and He, and $\delta^{13}C_{CO2}$ of near to 0‰
139 versus PDB. The fumaroles at Vulcano Porto have low emission temperatures (<100°C) and
140 compositions that are more typical of hydrothermal systems rich in H_2O, CH_4, and H_2S, and more
141 positive values of δD_{H2O} (Capasso et al., 1997; Nuccio et al., 1999, 2001; Paonita et al., 2002, 2013;
142 Granieri et al., 2006). The geochemical and isotopic compositions of these gas emissions underwent
143 large fluctuations during the last century reflecting potential volcanic unrest. There was an
144 important period of anomalous degassing during 1988–1993, which saw intensification of the
145 output rate of magmatic gases and expansion of the fumarole field that was coupled to the
146 temperature of the fumarolic fluids increasing to 690°C (Italiano et al., 1998). Similar events,
147 although minor in extent, occurred in 1996, 1998, 2004-2005, and 2009 (Granieri et al., 2006;
148 Paonita et al., 2013).
149
150 **3. Sample descriptions and laboratory techniques**
151 *3.1 Rock samples*
152 The analyzed products consist of eight lavas and tephra samples selected to cover the main stages of
153 activity at Vulcano and the different evolutionary degrees of the rocks (De Astis et al., 2006).
154 Generally, noble gas studies are performed on mafic minerals since they tend to retain the volatiles
155 entrapped during their growth (e.g., Marty et al., 1994). We selected rock samples having highly

156 porphyritic textures and large amounts of pyroxenes and olivines. The locations of the analyzed
157 rocks are shown in Fig. 1, and they are described briefly as follows:

158 a) The Capo Grillo formation (CG sample) belongs to the Primordial Vulcano stage of activity;
159 it consists of porphyritic lava flows that erupted at ~110 ka, and has compositions varying
160 from basaltic-andesite to shoshonite (De Astis et al., 2006).
161 b) The Passo del Piano lava (PP sample) and La Sommata scoriae (SOM sample) erupted at 49
162 and 42 ka, respectively, and represent the infill products of the Piano Caldera. These
163 samples are the most-basic rocks of the island, with MgO >7 wt.% (Keller, 1980; De Astis
164 et al., 1997).
165 c) Piano Grotte dei Rossi (PGR sample) is a pyroclastic deposit generated from activity at the
166 La Fossa caldera at ~18 ka. This deposit is characterized by a massive matrix rich in augitic
167 clinopyroxenes larger than 1 cm, which probably derives from a crystal mush (Keller, 1980;
168 De Astis et al., 1997).
169 d) For the activity of the La Fossa cone during the last 1000 years, we selected the following
170 three rock samples with SHO and KS affinities: (1) rock samples from the porphyritic
171 latitic lava flow of the Palizzi-Commenda Eruptive Cycle (Di Traglia et al., 2013; PA
172 sample), with high contents of clinopyroxene phenocrysts and subordinate olivine, and
173 which erupted during the 12th and 13th centuries (Di Traglia et al., 2013); (2) latitic
174 enclaves within the rhyolitic lava flow of Pietre Cotte (PC sample, 1720±20 AD; Piochi et
175 al., 2009); and (3) ashes of the 1888–1890 AD eruption (88-90 sample), which are the
176 youngest products of the La Fossa cone investigated in this study.
177 e) Two lava samples were collected at Vulcanello peninsula: (1) a sample related to the
178 shoshonitic lava platform (VUL sample, 1100–1250 AD; Arrighi et al., 2006; Di Traglia et
179 al., 2013 and references therein) and (2) another belonging to the Roveto latitic lava flow
180 (ROV sample) that was emplaced during the 17th century.

181 *3.2 Analytical methods*

182 Micro-analytical data on clinopyroxene, plagioclase, olivine and oxide crystals were obtained on
183 polished thin sections at the Dipartimento di Scienze Biologiche, Geologiche e Ambientali,
184 University of Catania (Italy) using a Tescan Vega-LMU scanning electron microscope equipped
185 with an EDAX Neptune XM4-60 micro-analyzer operating by energy dispersive system
186 characterized by an ultra-thin Be window coupled with an EDAX WDS LEXS (wavelength
187 dispersive low energy X-ray spectrometer) calibrated for light elements. Operating conditions were
188 set at 20 kV accelerating voltage and 0.2 nA beam current for the analysis of major element

abundances on mineral phases. Repeated analyses on internationally certified augitic clinopyroxene, An-rich plagioclase, Fo-rich olivine, magnetite and glass inner standards during the analytical runs ensure precision for all the collected elements on the order of 3-5%.

Major-element analyses were performed at the Dipartimento di Scienze Biologiche Geologiche e Ambientali of the University of Catania (Italy) using an X-ray fluorescence spectrometer (Philips PW2404) on powder pellets with matrix-effect corrections according to Franzini et al. (1972). Loss on ignition (LOI) was determined by gravimetric methods and corrected for Fe^{2+} oxidation.

Trace-element analyses were performed using inductively coupled plasma mass spectrometry (ICP-MS) at the Istituto Nazionale di Geofisica e Vulcanologia (INGV), Sezione di Palermo. Samples were prepared using the procedure by Correale et al. (2014): the rock samples were crushed and powdered by an agate mortar, with a 0.1-g aliquot thereof being digested with HF and HNO_3. The analytical precision and accuracy were ≤10% and ≤5%, respectively, for most trace elements (see also Table 2S in the supplementary material online).

The Sr- and Pb-isotope compositions for the whole rock were measured at the NERC Isotope Geosciences Labs of the British Geological Survey in Nottingham (UK). 150–200 mg of sample powder was dissolved using HF and HNO_3. Following conversion to the chloride form, the samples were reconverted to nitrate prior to the separation of Sr and Pb using Sr-SPEC ion-exchange resin. Procedural blanks for Sr and Pb during the analysis period were <100 pg. Sr fractions were loaded onto outgassed single Re filaments using a TaO activator solution, and analyzed in a mass spectrometer (Triton, Thermo-Electron) in multidynamic mode. The data reported here are normalized to $^{86}Sr/^{88}Sr = 0.1194$. Eighteen measurements of the SRM987 Sr standard run across the time of sample analysis gave a value of 0.710253±0.000011 (mean±SD).

The Pb isotopes in the samples were analyzed using multiple-collector ICP-MS (Nu Plasma, Nu Instruments). Prior to the analysis, each sample was spiked with a Tl solution, which was added to allow for correction of instrument-induced mass bias. Samples were then introduced into the instrument via an ESI 50 µl/min PFA microconcentric nebulizer attached to a de-solvation unit (DSN 100, Nu Instruments). The precision and accuracy of the method was assessed through the repeated analysis of an NBS 981 Pb reference solution (also spiked with Tl). The average values obtained for each of the measured NBS 981 ratios were then compared with the known values for this reference (Thirlwall, 2002). All sample data were subsequently normalized according to the relative daily deviation of the measured reference value from the known true value.

The elemental and isotopic compositions of noble gases hosted in mineral fluid inclusions were analyzed by single-step crushing at INGV, Sezione di Palermo. Olivine and clinopyroxene (with size of 0.5–2.0 mm) were selected by hand picking under a binocular microscope and then

ultrasonically cleaned sequentially in 5% HNO_3, distilled water, and high-purity acetone (15 min for each). The weight of the samples ranges from 1.0 to 4.1 g; depending on the average dimension of the phenocrysts, each sample consists of a variable number of crystals (normally, a few hundreds). The crusher, which was capable of loading up to six samples simultaneously, was heated under pumping conditions overnight at 130°C in order to reach an ultrahigh vacuum (10^{-9} mbar). Samples were then crushed at room temperature. Before isotope analysis, helium and neon were separated from argon by adsorbing the latter in a charcoal trap cooled by liquid nitrogen (-196 °C). After then, helium and neon have been adsorbed in a cryogenic trap connected to a cold head cooled with a helium compressor at 10 K. Helium has been desorbed at 42 K and admitted into the Mass Spectrometer (MS). After restoring ultra-high-vacuum in the cryogenic trap, Ne was released at 82 K and then admitted in a distinct MS (both Helix SFT Thermo). Ar-isotope composition was determined using an Argus (GVI) mass spectrometer following procedures similar to those reported previously (e.g., Nuccio et al., 2008; Rizzo et al., 2015). Typical blanks had less than 10^{-15} mol of He and less than 10^{-14} mol of Ar.

4. Results

4.1 Petrography and whole-rock composition

4.1.1 Petrography

The analyzed volcanic products of Vulcano show differences in their petrographic features that are consistent with their bulk-rock composition. Overall they exhibit a seriate porphyritic texture with a variable porphyritic index ranging between 3 and 30 vol.% (Table 1). The mineral assemblage consists mainly of clinopyroxene (40–80 vol.%), plagioclase (0–55 vol.%), olivine (0–30 vol.%), and opaque oxides (<5 vol.%). Orthopyroxene is present as rare relicts in the SOM sample. The groundmass ranges from microcrystalline to cryptocrystalline in the most-evolved products (PA, and enclaves of PC samples) and in the PP basalts, hyalopilitic in La Sommata and Vulcanello products, and vitrophyric in those of the 1888–1890 eruption at the La Fossa crater. The mineralogical assemblage in the groundmass is similar to that of phenocrysts, with clinopyroxene and plagioclase as the dominant phases. Glomerophyric structures have been observed within the enclaves of Pietre Cotte, the lava flow of Palizzi, and the final products of the 1888–1890 eruption. These structures comprise plagioclase and clinopyroxene crystals (larger than 1 cm), subordinate olivine, and opaque oxides.

Among all of the considered volcanic products, clinopyroxene is the dominant mineralogical phase (up to 80 vol.%), with dimensions ranging from 0.5 to 5 mm and a euhedral to subhedral habitus. Direct correlations of crystal abundances with the stratigraphic sequence are not evident, at least for

257 the studied samples (Table 1). Clinopyroxene crystals in the analyzed samples are augitic in
258 composition with ranges of $Wo_{33-47} - En_{42-62} - Fs_{5-15}$ at the cores and $Wo_{35-47} - En_{42-60} - Fs_{5-14}$ at the
259 rims (Table 1S in the supplementary material online). Plagioclase crystals are more abundant (up to
260 55 vol.%) in the most-evolved eruptions, such as those of Palizzi and Pietre Cotte, whereas they are
261 lacking in Passo del Piano products (Table 1). The c-axis of plagioclase phenocrysts is up to 6 mm
262 long, although the most-frequent length is 0.5–2 mm. Plagioclase xenocrysts, which are widely
263 found in most of the samples, show resorbed cores and dissolution textures. Plagioclase cores range
264 between bytownite and andesine in composition (An_{71-43}), whereas rims are more evolved, from
265 labradorite to albite (An_{58-6}; Table 1S in the supplementary material online). It is worth noting that
266 plagioclase outer rims in ROV and PC samples are overgrown by a K-feldspar envelope. Olivine
267 generally occurs as euhedral to subhedral phenocrysts with frequent rims of iddingsite due to post-
268 emplacement alteration.
269 The size of phenocrysts generally varies between 0.5 and 1.5 mm, with only a few crystals reaching
270 4 mm. In general, olivine is a subordinate mineralogical phase among mafic crystals, constituting
271 less than 10 vol.% (except for Passo del Piano products where its content is up to 30 vol.%). The
272 forsterite content of the analyzed olivines ranges between Fo_{81}, recorded in crystals of the PP
273 sample, and Fo_{57} of the PA sample (Table 1S in the supplementary material online). Opaque oxides
274 do not show marked variability and can be classified as titaniferous magnetite. TiO_2 concentration
275 is generally at 7-8 wt.% in all the samples, except for the PP sample (~13 wt.%; Table 1S in the
276 supplementary material online).
277 Petrographic observations and mineral chemistry data show that almost all analyzed phenocrysts
278 have a primary signature. Indeed, their compositions are compatible with those of hosting whole
279 rock, and their outer parts do not show dissolution and/or resorption textures due to geochemical
280 disequilibrium between melt and crystal. Furthermore, there is a narrow compositional variability of
281 crystals among each studied eruptive event and only a very small percentage of them (< 1 wt.%)
282 seem to be xenocrysts and/or antecrysts, that are typically characterized by an anhedral habit due to
283 dissolution/resorption. Mineral phases, and their hosted fluid inclusions, can be therefore considered
284 as essentially representative of the magmas from where they crystallized.
285
286 *4.1.2 Major and trace elements*
287 There have been numerous geochemical and petrologic studies of the products emitted at Vulcano
288 (Keller, 1980; Clocchiatti et al., 1994b; De Astis et al., 1997; Del Moro et al., 1998; Gioncada et al.,
289 1998, 2003; Davì et al., 2009a,b); the present results (see Table 2) are comparable to those
290 previously obtained. The analyzed samples plotted in the Total Alcali Silica (TAS) diagram in

Fig. 2 display variable compositions from basalt to trachyte. The more-basic and ancient rocks studied here (PP and SOM samples) belong to the HKCA-SHO series, while the other samples have high K_2O content (>3 wt.%), with SHO and KS affinities and variable SiO_2 contents. This is in accord to the magmatism of the island characterized by a progressive increase in K_2O over time (Keller, 1980; De Astis et al., 1997). Generally, the variations in both the major and trace elements versus SiO_2 follow a fractional crystallization trend, with negative correlations for ferromagnesian elements and positive correlations for incompatible elements (Fig. 3). However, the PC and 88-90 samples show a linear array with a wide compositional variability, which has been attributed by several authors to mixing or mingling processes between latitic and rhyolitic end-members (De Astis et al., 1997, 2000, 2013; Del Moro et al., 1998).

The analyzed rocks show similar patterns (Fig. 4), with fractionation of heavy rare-earth elements (HREE) and different degrees of enrichment in large-ion lithophile elements (LILE) (Rb, Sr, Cs, Th, U, and Pb) and light rare-earth elements (LREE) (particularly La and Ce; Keller, 1980; De Astis et al., 1997, 2000, 2013; Del Moro et al., 1998; Peccerillo et al., 2013). A geochemical feature common to all of the samples is depletion of the high-field-strength elements (HFSE), as testified by negative anomalies of Nb, Ta, and Ti.

The concentrations of the incompatible elements increase with the SiO_2 and K_2O contents except for Ba, Sr, and Eu, which are removed by plagioclase and K-feldspar fractionation under low-pressure conditions in the younger and more-evolved rocks (De Astis et al., 1997; Del Moro et al., 1998; Gioncada et al., 1998; Schiano et al., 2004). The products younger than 30 ka (belonging to the SHO-KS series) are more enriched in incompatible elements than are the ancient HKCA-SHO volcanic rocks. These younger products have also higher Rb/Zr, Th/Yb, Th/La, and La/Sm values (Francalanci et al., 2007; De Astis et al., 2013; Peccerillo et al., 2013). The mechanism underlying the production of magma that becomes progressively enriched in K_2O and incompatible elements is still debated. Some authors have suggested that the KS series originate from a metasomatized residual lithospheric source with respect to the HKCA-SHO melts from the asthenospheric region (Keller, 1980; De Astis et al., 1997, 2000). Other authors have proposed that the magmatic source has not changed over time, and that the production of KS magmas is due to lower degrees of partial melting as indicated by La/Sm in the mafic rocks, which increases with K_2O content (Peccerillo et al., 2013). Moreover, assimilation and fractional crystallization combined with refilling and tapping processes could lead to enrichment of K_2O and incompatible elements (Del Moro et al., 1998; Francalanci et al., 2007).

4.1.3 Sr and Pb isotopes

The Sr- and Pb-isotope compositions of whole rocks were determined for some key samples. As presented in Table 3, $^{87}Sr/^{86}Sr$ ranges between 0.704287 and 0.704697. The SOM sample shows the least-radiogenic Sr isotope composition, whereas the other samples—from the last 2 ka of activity—have comparable or higher Sr-isotope ratios despite their different extents of evolution. The ranges for Pb isotopes are 19.400–19.590, 39.345–39.415, and 15.692–15.703 for $^{206}Pb/^{204}Pb$, $^{208}Pb/^{204}Pb$, and $^{207}Pb/^{204}Pb$, respectively. The SOM sample displays higher values than the other samples, except for similar values of $^{207}Pb/^{204}Pb$ (Table 3; Fig. 5). There is a wide variability of these isotope ratios in the literature, and our results fall in the range from previous studies (Clocchiatti et al., 1994b; De Astis et al., 1997; Del Moro et al., 1998; Gioncada et al., 1998, 2003) (Fig. 5). Several authors have attributed these wide ranges to processes of crustal assimilation of the Calabrian basement (De Astis et al., 1997; Del Moro et al., 1998; Frezzotti et al., 2004), a feature confirmed by Sr-isotope ratios (Fig. 5). However, minor deviations from the trend expected by the sole assimilation of a Calabrian basement could also be related to involvement of other isotopically distinct components (i.e., sedimentary) in the mantle source of magmas as also observed in other volcanoes of Southern Italy (Viccaro et al., 2011; Correale et al., 2014).

4.2 Isotopic composition of noble gases in fluid inclusions

Isotope data for noble gases, which were obtained by crushing crystals of olivine and pyroxene, are reported in Table 4. The noble gases are good tracers of deep magmatic fluids due to the large contrast in the elemental and isotopic compositions between mantle, crust and atmosphere. For the same reason, their original composition in fluid inclusions can be susceptible to secondary changes due to entrapment of atmospheric components in mineral microcracks or during sample preparation (Marty et al., 1994; Ballentine and Barfod, 2000). Given that Ar and Ne are more abundant in the atmosphere (9340 and 18 ppm, respectively) with respect to magmatic gases, the effects of the air contribution are more evident for $^{40}Ar/^{36}Ar$ and $^{4}He/^{20}Ne$. $^{40}Ar/^{36}Ar$ varies between 295.5 and 342.3, while $^{4}He/^{20}Ne$ varies between 0.3 and 165.7. Both of these isotope ratios are well below those of the typical MORB source ($^{40}Ar/^{36}Ar$ = 30000–40000 and $^{4}He/^{20}Ne \geq 1000$; Burnard et al., 1997), suggesting that all of the present samples were contaminated by air at some extent.

The He concentration and isotope ratio of fluid inclusions are plotted in Fig. 6. $^{3}He/^{4}He$ is expressed in Rc/Ra, which is the He-isotope ratio of the sample corrected for the air contamination and normalized to the air value ($^{3}He/^{4}He_{air} = 1.39\times10^{-6}$). The atmospheric contribution to $^{3}He/^{4}He$ was evaluated using the method of Sano and Wakita (1988), which utilizes $^{4}He/^{20}Ne$. The corrected $^{3}He/^{4}He$ does not virtually differ from uncorrected values for most of the samples, while only a minor effect is noticed for augite separates of PA, VUL and ROV. Most of the analyzed products

have He concentrations ranging between 10^{-14} and 10^{-13} mol/g. In contrast, $^{3}He/^{4}He$ shows variable values ranging from 3.30 R/Ra (for VUL olivines) up to 5.94 R/Ra (for SOM olivines). The He-isotope ratios are not available for all of the crushed mineral samples (Table 4) since the amount of ^{3}He in fluid inclusions was sometimes lower than our detection limit. There are few $^{3}He/^{4}He$ data from fluid inclusions in the Vulcano island literature (Magro, 1997; Martelli et al., 2008). Our values are in overall agreement with those of Martelli et al. (2008), which vary between 2.29 and 4.84 R/Ra. Samples of our collection directly comparable to those of Magro (1997) show a good agreement.

5. Discussion

5.1 Variation of $^{3}He/^{4}He$ in rock samples

Mineral chemistry has highlighted that the more primitive the magmas, the more primitive the mafic mineral phases (see Sect. 4.1.1). Consequently the entrapped fluid inclusions in olivines and pyroxenes can be equally considered as representative of the crystallizing melt. Thus it is not surprising that the He isotope ratios of our samples show a broadly inverse correlation with the degree of evolution of the rocks (Figs. 7a and b), with the exception of ROV which has anomalously high $^{3}He/^{4}He$ ratios. The highest measured He isotope values (SOM and ROV samples) fall in a range compatible with the $^{3}He/^{4}He$ marker of the deep magmatic source beneath Vulcano, which has been constrained to be equal or higher than 6.0 R/Ra on the basis of geochemical studies on the fumarolic fluids (Tedesco, 1995; Italiano and Nuccio, 1997; Magro, 1997; Tedesco and Scarsi, 1999; Taran, 2011). Given that the highest R/Ra ratios have been observed in different stages of the volcanic activity (~6 R/Ra from SOM, ROV and present fumaroles; Fig. 7c), we can infer that the isotope marker of the source of Vulcano magmas has remained homogeneous over time.

It is worth noting that the maximum values of $^{3}He/^{4}He$ in fluid inclusions and fumaroles in Vulcano are lower than values usually attributed to MORB (8±1 R/Ra; Hilton et al., 2002) and also distinctly lower than the most primitive values of the Italian active volcanism recorded in volcanoes of the Sicilian area (e.g., Etna, 7.6 R/Ra, Pantelleria, 7.3 R/Ra; Correale et al., 2014, Parello et al., 2000). With regard to the Aeolian Islands, the maximum helium isotope values are recorded in the westernmost islands (in particular in Alicudi, 7.1 R/Ra; Martelli et al., 2008). The shift toward more crustal-contaminated compositions when proceeding eastward in the Aeolian islands and northward along the whole Italian volcanic province leads to very low helium isotope ratios, in both free gases and fluid inclusions in mafic phenocrysts (i.e., ~1 R/Ra in Vulsini volcanoes, Latium). This general $^{3}He/^{4}He$ trend corresponds to a wide increase in $^{87}Sr/^{86}Sr$ and a decrease in $^{143}Nd/^{144}Nd$ and

$^{206}Pb/^{204}Pb$, and has been attributed to progressively increasing mantle wedge contamination due to the subduction of the Ionian-Adriatic slab (Marty et al., 1994, Martelli et al., 2004, 2008). He, Sr and Pb isotopes measured in Vulcano rocks therefore show that the mantle source of this island is close to the most primitive compositions of the region, but they have undergone some contamination effects due to the mantle wedge enrichment via the Ionian subduction.

In addition to the two samples displaying He isotopes matching the magmatic source of Vulcano (SOM and ROV), the other volcanic rocks investigated have lower $^{3}He/^{4}He$ values, with average values between 5 and 4 R/Ra. Several processes could be responsible for the observed variability in the He-isotope ratio of our samples. For example, $^{3}He/^{4}He$ could have decreased in fluid inclusions during the storage and evolution of the magma in crustal reservoirs, before the eruptive event (Marty et al., 1994; Hilton et al., 2000, 2002). Also, after their emission, phenocrysts might not preserve the original magmatic isotope ratios due to the presence of several post-depositional processes that are discussed below.

5.1.1 Post-eruptive processes

$^{3}He/^{4}He$ measured in fluid inclusions of Vulcano might be sensitive to post-eruptive modifications due to ^{4}He radiogenic ingrowth associated with U and Th decay inside the mineral lattice. The U and Th concentrations inside phenocrysts have been calculated based on the concentrations of these elements in the whole rock taking into account that the partition coefficient between mineral and melt is 0.01 for pyroxene and 10^{-4} for olivine (McKenzie and O'Nions, 1991). The amounts of ^{4}He produced in pyroxenes and olivines since the eruptive event were then calculated. The results give an amount of radiogenic He that is two to three orders of magnitude lower than the He concentration measured in mineral samples, which would have negligible effects on $^{3}He/^{4}He$. Only for the PP pyroxenes was the amount of *in-situ* radiogenic He comparable to the measured values. Theoretically, ^{4}He radiogenic ingrowth for these PP minerals could have modified the original isotope ratio. However, since the crushing technique used in the present study minimizes the release of the reticular He produced inside the crystal matrix, the level of radiogenic He should be orders of magnitude higher than that of the entrapped He in order for the latter to be affected. Accordingly, the isotope ratios of the PP sample are within the range of other more-recent rocks of Vulcano.

Another process that is able to decrease $^{3}He/^{4}He$ in mafic phenocrysts is the diffusive fractionation of the two He isotopes due to their different diffusivities from the crystal (Harrison et al., 2004). Nuccio et al. (2008) invoked this process to explain $^{3}He/^{4}He$ being lower in pyroxene-hosted fluid inclusions than in cogenetic olivine crystals at Mt. Etna. In our case, olivine and pyroxene crystals do not show any systematic variation of the type found for Mt. Etna products. In some rock samples

427 the cogenetic mineral pairs show an opposite behavior, with $^3He/^4He$ being higher in pyroxene and
428 lower in olivine (e.g., VUL and SOM samples). Furthermore, there is no clear trend of concordant
429 $^3He/^4He$ and He content decreases (Fig. 6), as expected in the case of diffusion (Harrison et al.,
430 2004). We therefore believe that diffusive fractionation is not the process responsible for the
431 decrease in $^3He/^4He$ in the Vulcano products.
432 One post-eruptive process that is able to increase the He-isotope ratio is cosmogenic ^3He ingrowth
433 inside the crystal lattice due to exposure of the rock to cosmic rays (Lal, 1991; Sarda et al., 1993;
434 Brent et al., 2010). The effects of ^3He cosmogenic production are directly dependent on the latitude
435 and altitude of rocks (Lal, 1991) together with their rate of erosion, because ^3He production is
436 effective down to a depth of 50 cm (Sarda et al., 1993). In order to reduce the effects of cosmogenic
437 production, only rocks near to active cliffs or in recent excavation walls were sampled, so as to
438 minimize time of exposure. Moreover, the crushing technique employed greatly reduces the release
439 of the cosmogenic ^3He (as for all reticular components), ruling out potential effects of cosmogenic
440 ^3He production on $^3He/^4He$.
441
442 *5.1.2 Pre-eruptive processes: influence of crustal ^4He*
443 Rocks of Vulcano Island are characterized by different $^3He/^4He$ values even when they have
444 undergone the same degree of evolution. A well-known process that can lower the $^3He/^4He$ ratio
445 may be the accumulation of radiogenic ^4He produced by alpha decay of U and Th dissolved in
446 magma (which is known as "magma aging"). Assuming that $^3He/^4He$ is 6.2 R/Ra for the deep
447 magmatic source of Vulcano for all products (Magro, 1997; Tedesco and Scarsi, 1999; Taran, 2011)
448 and considering the U and Th concentration in each sample, it is possible to calculate the time that
449 would be required to produce the amount of radiogenic ^4He needed to decrease $^3He/^4He$ from the
450 pristine magma directly derived from the source to the measured values. In this calculation, the final
451 He-isotope ratio depends on the initial amount of He in the pristine magma.
452 By fitting a degassing model to the fumarole compositions, Paonita et al. (2013) constrained the He
453 concentration in degassing magmas to be around 10^{-10} mol/g of basaltic and shoshonitic melts,
454 whereas latitic and trachytic melts would contain 1.5×10^{-11} mol/g He. By assuming the He isotope
455 values of SOM and ROV as largely unaffected by processes changing the magmatic source
456 signature, the estimated residence times required to decrease the R/Ra from the source value to the
457 analyzed value in the other samples move in the range 45 to 1900 ka. These times are unfeasibly
458 long when compared to the eruptive history of the subaerial portion of Vulcano Island (120 ka), and
459 hence this process cannot explain the large $^3He/^4He$ variations observed in the rocks. Other
460 processes therefore need to be identified to explain the decrease in $^3He/^4He$ in the volcanic rocks.

461 Various authors have proposed that the Vulcano magmas have been subject to crustal assimilation
462 processes of the metamorphic Calabrian basement (De Astis et al., 1997, 2000, 2013; Del Moro et
463 al., 1998; Frezzotti et al., 2004; Francalanci et al., 2007). For volcanic arcs emplaced on the
464 continental crust, some authors have proposed that a decrease in $^{3}He/^{4}He$ of emitted products can be
465 ascribed to assimilation of ^{4}He-enriched crust (Hilton et al., 2002; Van Soest et al., 2002; Shimizu
466 et al., 2005; Shaw et al., 2006). In order to explain the low $^{3}He/^{4}He$ of most of our samples, we
467 tested the hypothesis of assimilation of a crustal component from the Calabrian-like basement into
468 magmas stored in the magmatic system of Vulcano.
469 Data on the elemental and isotopic compositions of He in the Calabrian basement can be used to
470 determine the effects of crustal ^{4}He assimilation on $^{3}He/^{4}He$ values in magmas. He in the basement
471 is of radiogenic origin (Bach et al., 1999), which means that its isotopic composition can be
472 constrained to the typical crustal value of 0.05 R/Ra (Ozima and Podosek, 1983). The amount of He
473 in rocks of the Calabrian basement is proportional to the U and Th concentrations in the same rocks,
474 whose average values are 2.7 and 11 ppm, respectively (Caggianelli and Prosser, 2001). Since the
475 Calabrian basement comprises Hercynian metamorphic rocks, the amount of radiogenic He
476 produced in the crustal basement after the last metamorphic event can be derived (Bach et al.,
477 1999), based on the fact that noble gases trapped in rocks are entirely lost during metamorphic
478 processes (Lippolt and Weigel, 1988; Bebout and Fogel, 1992). Hercynian metamorphism is
479 commonly considered to have ended at the end of the Permian period, giving an estimated ingrowth
480 time of 250 Myr. With these constraints, the amount of radiogenic ^{4}He produced in the crust is
481 estimated as 7×10^{-9} mol/g of rock. However, the high diffusivities of He isotopes mean that the
482 continental crust is exposed to significant natural degassing over time, which is greater in the upper
483 crust where tectonic structures facilitate He release (Bach et al., 1999; Hoke et al., 2000). Bach et
484 al. (1999) studied the variations of He and Ar concentrations for metabasitic and metapelitic rocks
485 along a 7-km-deep borehole, and observed that 80–95% of the He is lost by diffusion at shallow
486 levels. Considering that the Calabrian basement should be located between depths of 7 and 2 km
487 (Peccerillo et al., 2006), we assume that the continental crust lost 80% of its radiogenic ^{4}He,
488 yielding a final He concentration equal to 1.5×10^{-9} mol/g of rock. This value is comparable with the
489 He concentration determined analytically by various authors for the continental crust (Allègre et al.,
490 1986; Marty et al., 1994; Bach et al., 1999).
491 Assuming that all of the He contained in assimilated crustal rocks is dissolved into the magma
492 body, we can estimate that the assimilation of 25% of the crustal basement (with 0.05 R/Ra) could
493 reduce the He-isotope ratio from 6.2 to 3.4 R/Ra, which is the most-contaminated isotope value in
494 our data set. This is in accordance with previous suggestions that the assimilation of 8–30% of the

crustal component could explain the chemical features of the Vulcano magmas (De Astis et al., 1997; Del Moro et al., 1998; Frezzotti et al., 2004; Francalanci et al., 2007). Despite uncertainty about the validity of the approximations used, the assimilation of 10–25% of the crustal component into melts in the plumbing system provides a satisfactory explanation of the low $^{3}He/^{4}He$ values of the samples with respect to the pristine magma from the mantle source.

5.1.3 $^{3}He/^{4}He$ versus $^{87}Sr/^{86}Sr$ relationships: assimilation of the Calabrian crust

Many authors have used correlations between He and Sr isotopes to evaluate the effects of subduction and crust contamination on $^{3}He/^{4}He$ in various volcanic systems (e.g., Hilton et al., 1992; Marty et al., 1994; Van Soest et al., 2002). Fig. 8 compares $^{3}He/^{4}He$ values of the samples with measured $^{87}Sr/^{86}Sr$ values of whole rocks (for PP, CG, and PGR samples, with the Sr-isotope data obtained from the literature; De Astis et al., 1997; Del Moro et al., 1998). Given that assimilation of the crustal component into magmas is the most likely explanation for the low $^{3}He/^{4}He$ values, we modeled the effects of this process on the Sr elemental and isotopic compositions by mixing the crustal material to the magmatic melt.

The Sr isotopic and elemental compositions of the pristine uncontaminated magma coming from the mantle source and of the Calabrian crust are needed to evaluate the effect of assimilating the latter into the former. Opinions differ as to the composition of the deep source of Vulcano that generates the pristine magma. Some authors have suggested that the magmatic source changed at about 30 ka (De Astis et al., 1997, 2000), while other authors consider that magmas were produced by different degrees of melting of a time-constant and homogeneous source (Del Moro et al., 1998; Francalanci et al., 2007; Peccerillo et al., 2013). For this reason, the assimilation process was analyzed in the present study for both cases. Regarding the crustal end-member, we have assumed that the Calabrian crust has an average $^{87}Sr/^{86}Sr$ of 0.72505 (De Astis et al., 1997; Del Moro et al., 1998; Frezzotti et al., 2004) and an Sr-element concentration of 126 ppm (Caggianelli and Prosser, 2001). The mixing parameters for He are given in Section 5.1.2.

The case of two pristine magmas generated by two different mantle sources is reported in Fig. 8a (referred to as two-sources model). According to De Astis et al. (2013), a less-radiogenic source ($^{87}Sr/^{86}Sr \sim 0.70414$) would have fed the eruptive activity before 30 ka, whereas a slightly more radiogenic source ($^{87}Sr/^{86}Sr \sim 0.7045$) would have generated magmas that characterize the post-30-ka eruptions. These values can be selected as representative of the two different magmatic end-members. In both end-members we have considered an initial Sr concentration equal to that of the more-primitive rocks that erupted at the island, namely that of the SOM sample. The mixing curve for each magmatic end-member was derived by applying the initial He concentration in the

magmatic source (10^{-10} mol/g, see above) as determined by Paonita et al. (2013). Considering that this value could be due to the magma already being partially degassed relative to a primitive one, we investigated the effects of He contents up to 5×10^{-10} mol/g.

Fig. 8a shows that the decrease in $^{3}He/^{4}He$ is proportional to the percentage of crustal assimilation, whereas the slope of the curves mainly depends on the initial He concentration. Indeed, a given amount of crustal assimilation causes decreases in $^{3}He/^{4}He$ for magma having a low initial He concentration (10^{-10} mol/g) that are larger than those for magmas with higher He contents. The mixing curves provide a good fit to the analyzed products with the exception of the CG and ROV samples. In this regard, the CG sample is the oldest rock studied here (>30 ka) together with the PP and SOM samples, but it does not fall on the mixing curve related to the older source (gray dashed lines) due to the He-isotope ratio being higher than $^{87}Sr/^{86}Sr$. This feature can also be observed for the younger ROV sample (<30 ka) that is different from other rock samples and from the mixing curves of the post-30-ka source, in that it has an anomalously high $^{3}He/^{4}He$.

Fig. 8b presents the case of a single pristine magma coming from a homogeneous mantle source (single-source model). In this case, assuming a magmatic end-member with $^{87}Sr/^{86}Sr$ ranging between 0.70415 and 0.70429 and the Sr content of SOM, all of the rock samples fall along or close to the mixing lines. Even in this case the ROV sample—and partially also the CG one—represents an outlier, being characterized by a high $^{3}He/^{4}He$ relative to its Sr-isotope composition and evolutionary degree.

The ROV latite therefore has anomalously high $^{3}He/^{4}He$ values regardless of whether a single-source or a two-source mixing model is used. It should also be noted that in the two-source case the CG shoshonite also departs from the crustal assimilation trend assumed for the pre-30-ka source. However, the ROV and CG samples display high Sr-isotope ratios that suggest they were affected by contamination processes associated with continental crust assimilation, as demonstrated by petrochemical studies (De Astis et al., 1997; Del Moro et al., 1998; Frezzotti et al., 2004; Francalanci et al., 2007). A consistent indication comes from a comparison of $^{3}He/^{4}He$ values with Pb-isotope ratios (see Table 3, figure not shown), where the ROV sample departs from the trend expected for crustal assimilation because it has higher $^{3}He/^{4}He$ values than the other rocks, despite similar Pb-isotope values (see Section 4.1.3). The next section explores the reasons why the ROV sample is peculiar among the Vulcano rocks.

5.2 Magma flushing by volatiles

Explaining the higher $^{3}He/^{4}He$ observed particularly in the ROV sample with respect to Sr and Pb isotopes requires a further process that supplies He with a high $^{3}He/^{4}He$ without also carrying

563 significant amounts of Sr and Pb into the magmatic body. The most-plausible candidate could be
564 the migration of H_2O- and CO_2-rich fluids coming from magma degassing throughout the plumbing
565 system. The affinity of He to these supercritical fluids is even higher than that of mobile elements
566 such as LILE (e.g., Rb, Ba, and Sr). Shallow reservoirs in the continental crust could therefore be
567 exposed to flushing by magmatic fluids rich in He with a high $^3He/^4He$ coming from the deepest
568 reservoirs. The flux of volatiles could in this way increase the He-isotope ratio of the magma body
569 without changing the Sr- and Pb-isotope ratios. Similar flushing models have previously been
570 hypothesized for Vulcano (Paonita et al., 2013) and also for other volcanic systems (e.g., at Mt.
571 Etna; Mazziotti Tagliani et al., 2012; Nicotra and Viccaro, 2012). Petrological and seismological
572 studies have revealed that the Vulcano plumbing system comprises two deep levels with pressures
573 of 500 and 300 MPa where magma is stored, and a main shallow reservoir with a pressure of ~100
574 MPa, at the density barrier between felsic granulites and Calabrian metapelites (~5 km deep; De
575 Astis et al., 1997, 2013; Zanon et al., 2003; Peccerillo et al., 2006).
576 Decompression of magmas during their ascent toward the shallow chambers induces crystallization,
577 which in turn generates lati-trachytic and rhyolitic melt compositions. The combined effect of
578 decompression and crystallization leads to the saturation of volatiles in the ascending magmas and
579 consequently to massive outgassing of fluids. The deep and primitive fluids moving toward surface
580 contain large amounts of He due to the low solubility of He in silicate melts (Iacono Marziano et al.,
581 2010), with a high $^3He/^4He$. Also they contain much less Sr than He, and they are able to flush
582 shallower magma bodies and to affect their abundances of ^3He and ^4He.
583 In addition to the above considerations, Vulcano magmas can evolve in small and sometimes
584 isolated reservoirs having sill- and dyke-like structures that are present at shallow levels of the
585 plumbing system (Chiarabba et al., 2004; De Astis et al., 2013; Paonita et al., 2013). This means
586 that each magma batch evolves and assimilates crustal rocks in different proportions depending on
587 various factors, such as its residence time, the geometry of the reservoir, and temperature. These
588 magmatic bodies could then be exposed to different degrees of flushing by deep fluids depending
589 on their location and shape. Small and evolved bodies, especially if they intrude as dykes, could
590 remain separate from the main pathways of fluid ascent and move toward low $^3He/^4He$ and high
591 $^{87}Sr/^{86}Sr$ values along the mixing curves in Fig. 8a and b. A typical example is the latitic enclaves in
592 the Pietre Cotte lava flow (our PC sample), testifying a dyke-shaped latitic body disrupted by a
593 rhyolitic melt during the eruption (Piochi et al., 2009). Similar magma batches—which are in
594 general largely degassed—will not erupt until they interact with other volatile-richer magmas. In
595 contrast, these bodies would exhibit dramatic changes in their He-isotope composition when flushed
596 by the He-rich deep fluids, especially since their previous degassing has removed some fraction of

He. In the case of ROV latite, although it has similar composition and Sr-isotope ratio to the PC sample, it displays much higher $^3He/^4He$ than predicted by the crustal assimilation models (Fig. 8). In this stage, the growing mineral phases entrap pristine volatiles coming from deep flushing, causing the $^3He/^4He$ to increase in fluid inclusions. Even for fluid inclusions entrapped in minerals prior to the flushing event, the complete diffusive He loss over hours to days measured for 0.5 mm olivine and pyroxene grains at magmatic temperatures (Trull and Kurz, 1993) suggests their re-equilibration with the flushing gases (both dissolved in melt and spread as bubbles) and complete obliteration of the original He isotope signature.

As a whole, the low $^3He/^4He$ in erupted rocks can be mainly attributed to assimilation processes of crustal Calabrian basement that would be the most-common condition at Vulcano, as testified by most of our samples. More rarely, the stored shallow bodies intercept fractures that are preferential pathways for fluid migration toward the surface, and they can be flushed by deep fluids characterized by high $^3He/^4He$. The ROV and CG samples indicate that this process has occurred throughout the volcanic record of Volcano and in magmas at various evolutionary degrees.

5.3 $^3He/^4He$ in rocks versus fumarolic gases: the present-day degassing magma

How the type and location of degassing magmas are related to the source of the fumarolic fluids emitted at the La Fossa crater can be established by comparing the He-isotope ratio of the main magma compositions with that of the fumarolic gases (Fig. 6). Data on the He-isotope ratio of Vulcano fumaroles, which have been recorded for the past 25 years, indicate that fumarolic gases display $^3He/^4He$ values within the range of 4.8–6.2 R/Ra, and show large temporal fluctuations (Tedesco and Nagao, 1996; Italiano and Nuccio, 1997; Paonita et al., 2013). The lowest values (R/Ra < 5.2) are typical of fumarolic gases with very low contents of CO_2, He, and N_2, and generally low emission temperatures. These characteristics have been related to the contribution of fluids from a hydrothermal system residing beneath La Fossa (Capasso et al., 1997; Nuccio et al., 1999, 2001; Paonita et al., 2002, 2013). Paonita et al. (2013) constrained the typical magmatic end-member feeding fumaroles to be within the range of 5.2–6.2 R/Ra (shadow area in Fig. 6).

Fig. 6 shows that only the SOM and ROV samples have $^3He/^4He$ values comparable with fumarolic fluids, whereas a net decoupling between gas emissions and fluid inclusions is evident for the other rock samples. Moreover, the 88-90 samples have $^3He/^4He$ values that are lower than those of the gas emissions. Fumarolic gases therefore have a He-isotope ratio that is more representative of the deep magmatic source at Vulcano, with the exception of the SOM and ROV samples. Similar cases are documented in the literature for the Tabar, Lihir, Tanga, and Feni Islands in Papua New Guinea (Patterson et al., 1997), Canary Islands (Hilton et al., 2000), Irazu in Costa Rica (Shaw et al., 2006),

631 and Mt. Etna (Nuccio et al., 2008). This condition is not observed at nearby Stromboli Island, where
632 gases from both thermal aquifers and recent fluid inclusions have He-isotope ratios similar to those
633 of the primitive magma feeding the current paroxysmal activity (Martelli et al., 2014).
634 The last few decades have seen various attempts to determine the composition of the magma
635 feeding the present fumarole field of Vulcano. Clocchiatti et al. (1994a,b) suggested that the
636 fumarole activity originates from degassing of a magma whose composition is intermediate between
637 basalt and latite. Nuccio et al. (2001) and Paonita et al. (2002) proposed an acidic-intermediate
638 magma composition based on an outgassing model for the main gaseous species contained in
639 fumarolic fluids. The variation of $^{3}He/^{4}He$ in rocks at different evolutionary degree led Magro
640 (1997) to hypothesize that the magmatic source of gas emissions is a basalt that is very similar to
641 that at La Sommata.
642 More recently, Paonita et al. (2013) studied the effects of silicate melt compositions on the
643 chemistry of an exsolved gas phase in the system H_2O-CO_2-N_2-He-$\delta^{13}C$. Cross-fitting of that model
644 with La Fossa fumarole compositions prompted Paonita et al. (2013) to propose the existence of a
645 latitic reservoir feeding the fumaroles at the crater. These authors coupled H_2O contents in melt
646 inclusions to the maximum CO_2 concentration in fumaroles to achieve an initial degassing pressure,
647 and they accordingly constrained by their degassing model the exsolution pressures of the fumarolic
648 gases and then the depth of the latite body. Such depth was estimated to extend in the range of 3.0–
649 3.5 km b.s.l. (Paonita et al., 2013), consistent with geophysical and structural evidence (Peccerillo
650 et al., 2006). According to Paonita et al. (2013), the large range of $^{3}He/^{4}He$ of the magmatic end-
651 member feeding the fumaroles (5.2–6.2 R/Ra) is likely to be due to mixing between fluids coming
652 from at least two ponding levels of magma which would form the latitic reservoir.
653 Based on the present results, only the SOM basalt and ROV latite had $^{3}He/^{4}He$ values comparable
654 to the He-isotope ratio of the magmatic end-member in the fumaroles. Taking into account that the
655 ROV sample corresponds to the most-recent eruption at Vulcanello (17th century; Fusillo et al.,
656 2015), whereas the SOM sample (~42 ka) is related to an old reservoir that has solidified (De Astis
657 et al., 2013), we believe that it is most likely that the magma feeding the present exhalative activity
658 has a latitic composition, and is stored in a small chamber that probably fed the last eruptive events
659 at Vulcanello. These conclusions are thus highly consistent with the results of Paonita et al. (2013).
660 This latitic reservoir, located at depths of 3.0–3.5 km, would not be able to sustain high gaseous
661 fluxes over a long period (Paonita et al., 2013), which is a key constraint to maintaining the
662 fumarole activity. When considering the total output from the fumarole field, the primary volatiles
663 in this latitic reservoir would in fact be exhausted within a few years (Inguaggiato et al., 2012).
664 Paonita et al. (2013) therefore invoked a periodic supply of more-primitive fluids (having a high

665 $^{3}He/^{4}He$) ascending from a deeper and more-voluminous magma reservoir located at a depth of
666 about 5 km (Peccerillo et al., 2006).
667 Within the framework of the present study, this process of gas flushing from a deeper reservoir
668 would be reflected by the high $^{3}He/^{4}He$ of the latitic ROV sample of Vulcanello (see Section 5.2).
669 The source of gas flushing would therefore be a basic magma that, in agreement with Peccerillo et
670 al. (2006), would be stored in the deepest parts of the reservoir at depths of ~5 km or in the magma
671 chamber whose top is located at a depth of about 8 km. The He-isotope ratio of the SOM basalt
672 (R/Ra = 5.94±0.16) may represent the most probable marker for fluids presently ascending from
673 this level. Furthermore, our findings imply that the greatest contribution to the high $^{3}He/^{4}He$ of the
674 ROV-like latite is flushing by fluids and not gas-carrying melts, since otherwise both $^{87}Sr/^{86}Sr$ and
675 the He-isotope composition of the latite would also have changed. The ingress of a more basic
676 magma from depths of 17–21 or 8–13 km (Peccerillo et al., 2006) into the shallower magma
677 reservoirs (at depths of 3–5 km) could occur only periodically, as testified by the widespread
678 presence of mingling textures in products emitted during the last 6 ka of activity at La Fossa
679 (Clocchiatti et al., 1994b; Piochi et al., 2009).
680
681 **6. Concluding remarks**
682 The main goal of the present study was to determine which type of magma presently feeds the
683 fumarole fields of the La Fossa cone. This objective was achieved by sampling rocks that had
684 undergone different degrees of evolution, and belonging to different stages of activity of Vulcano
685 Island. These new rock samples have been studied in three main ways, by determining (1) the
686 $^{3}He/^{4}He$ values of the fluid inclusions hosted in mafic minerals, (2) the bulk rock composition, and
687 (3) the Sr- and Pb-isotope compositions. The main findings of this study are as follows:
688 1. The analyzed rocks have compositions ranging from basalt up to trachyte and belonging to
689 HKCA-SHO and KS series. The Sr- and Pb-isotope ratios are all homogeneous except for
690 La Sommata basalt (SOM), which exhibits a less radiogenic Sr isotope ratio and higher Pb
691 isotope ratios.
692 2. The analyzed rocks have $^{3}He/^{4}He$ values ranging between 3.3 and 5.94 R/Ra. Only the SOM
693 basalts and the last-emitted latites of Vulcanello (ROV) have He-isotope ratios close to the
694 hypothetic source value for Vulcano (R/Ra = 6.0–6.2; Taran, 2011). The other rock samples
695 all have lower R/Ra ratios.
696 3. The decrease in $^{3}He/^{4}He$ in erupted rocks is mostly related to the assimilation of 10–25% of
697 the crustal component of the Calabrian basement, in agreement with petrological studies (De
698 Astis et al., 1997; Del Moro et al., 1998; Frezzotti et al., 2004). The identified correlations

between $^{87}Sr/^{86}Sr$ and $^{3}He/^{4}He$ values are consistent with an assimilation process, with the sole exception of the ROV sample that is characterized by high Sr- and He-isotope ratios. In this case, an input of deep magmatic fluids with high $^{3}He/^{4}He$ induces an increase in the He-isotope ratio without changing $^{87}Sr/^{86}Sr$.

4. The magmatic fluids presently feeding the fumarole field at Vulcano have $^{3}He/^{4}He$ values similar to those of the SOM and ROV samples. In accordance with Paonita et al. (2013), a latitic reservoir similar to the ROV sample probably represents the main magmatic source of the fumarole emissions. This latitic reservoir is periodically fed by deep fluids coming from basaltic magmas stored at deeper levels of the plumbing system and which are characterized by high $^{3}He/^{4}He$ values.

Acknowledgments

We thank A.L. Rizzo for performing the noble-gas analyses. L. Brusca, A. Correale, and M. Tantillo supported the noble-gas and trace-element analyses. V. Vashley carried out the Pb-isotope analysis. A. Di Piazza helped in sampling the La Sommata outcrop. Reviews by Christina Manning, an anonymous reviewer and the Editor A. Kerr are gratefully acknowledged. This study benefited from funding provided by Convenzione C DPC-INGV 2012.

References

Allègre, C.J., Staudacher, T., Sarda, P., 1986. Rare gas systematics: Formation of the atmosphere, evolution and structure of the Earth's mantle. Earth and Planetary Science Letters 81, 127–150. http://dx.doi.org/10.1016/0012-821X(87)90151-8

Arrighi, S., Tanguy, J.C., Rosi, M., 2006. Eruptions of the last 2200 years at Vulcano and Vulcanello (Aeolian Islands, Italy) dated by high-accuracy archeomagnetism. Physics of the Earth and Planetary Interior 159, 225-233. doi:10.1016/j.pepi.2006.07.010

Bach, W., Naumann, D., Erzinger, J., 1999. A helium, argon, and nitrogen record of the upper continental crust (KTB drill holes, Oberpfalz, Germany): implications for crustal degassing. Chemical Geology 160, 81–101.

Ballentine, C.J., Barfod, D.N., 2000. The origin of air-like noble gases in MORB and OIB. Earth and Planetary Science Letters 180, 39–48.

Bebout, G.E., Fogel, M.L., 1992. Nitrogen isotopic compositions of metasedimentary rocks in the Catalina Schist California. Geochimica et Cosmochimca Acta 56, 2139–2149.

Brent, M.G., Kurz, M.D., Balco, G., Schaefer, J.M., Licciardi, J., Lifton, N., 2010. A reevaluation of in situ cosmogenic ^{3}He production rates. Quaternary Geochronology 5, 410-418.

Burnard, P., Graham, D., Turner, C., 1997. Vesicle-specific noble gas analysis of popping rock: implications for primordial noble gases. Earth. Science 276, 568–571.

Caggianelli, A., Del Moro, A., Paglioncino, A., Piccarreta, G., Pinarelli, L., Rottura, A., 1991. Lower crustal granite genesis connected with chemical fractionation in the continetal crust of Calabria (southern Italy). European Journal of Mineralogy 3, 159-180.

Caggianelli, A., Prosser, G., 2001. An exposed cross-section of Late Hercynian upper and intermediate continental crust in the Sila nappe (Calabria, S. Italy). Periodico di Mineralogia 70, 277-301.

Cannata, A., Diliberto, S., Alparone, S., Gambino, S., Gresta, S., Liotta, M., Madonia, P., Milluzzo, V., Aliotta, M., Montalto, P., 2011. Multiparametric approach in investigating volcano-hydrothermal systems: the case study of Vulcano (Aeolian Islands, Italy). Pure and Applied Geophysics 169, 167–182. http:// dx.doi.org/10.1007/s00024-011-0297-z.

Capasso, G., Favara, R., Inguaggiato, S., 1997. Chemical features and isotopic gaseous manifestation on Vulcano Island (Aeolian Island): an interpretative model of fluid circulation. Geochimica et Cosmochimica Acta 61, 3425–3442. http://dx.doi.org/10.1016/S0016-7037(97)00163-4.

Chiarabba, C., Pino, N.A., Ventura, G., Vilardo, G., 2004. Structural features of the shallow plumbing system of Vulcano Island Italy. Bulletin of Volcanology 66, 477–484. http://dx.doi.org/10.1007/s00445-003-0331-9.

Chiodini, G., Allard, P., Caliro, S., Parello, F., 2000. ^{18}O exchange between steam and carbon dioxide in volcanic and hydrothermal gases: implications for the source of water. Geochimica et Cosmochimica Acta 64, 2479–2488. http://dx.doi.org/10.1016/S0016-7037(99)00445-7.

Clocchiatti, R., Gioncada, A., Mosbah, M., Sbrana, A., 1994a. Possible deep origin of sulfur output at Vulcano (Southern Italy) in the light of melt inclusion studies. Acta Vulcanologica 5, 49-53.

Clocchiatti, R., Del Moro, A., Gioncada, A., Joron, J.L., Mosbah, M., Pinarelli, L., Sbrana, A., 1994b. Assessment of a shallow magmatic system: the 1888-90 eruption Vulcano Island, Italy. Bulletin of Volcanology 56, 466–486.

Correale, A., Paonita, A., Martelli, M., Rizzo, A., Rotolo, S.G., Corsaro, R.A., Di Renzo, V., 2014. A two-component mantle source feeding Mt. Etna magmatism: Insights from the geochemistry of primitive magmas. Lithos 184-187, 243-258.

Davì, M., De Rosa, R., Donato, P., Vetere, F., Barca, D., Cavallo, A., 2009a. Magmatic evolution and plumbing system of ring-fault volcanism: the Vulcanello peninsula (Aeolian Islands, Italy). European Journal of Mineralogy 21, 1009-1028.

Davì, M., Behrens, H., Vetere, F., De Rosa, R., 2009b. The viscosity of latitic melts from Lipari (Aeolian Islands, Italy): inference on mixing-mingling processes in magmas. Chemical Geology 259, 89-97.

De Astis, G., Dellino, P., La Volpe, L., Lucchi, F., Tranne, C.A., 2006. Geological map of the island of Vulcano (Aeolian Islands). University of Bari, University of Bologna and INGV. LAC, Firenze.

De Astis, G., La Volpe, L., Peccerillo, A., Civetta, L., 1997. Volcanological and petrological evolution of Vulcano island Aeolian Arc, Southern Tyrrhenian Sea. Journal of Geophysical Research 102, 8021–8050.

De Astis, G., Lucchi, F., Dellino, P., La Volpe, L., Tranne, C.A., Frezzotti, M.L., Peccerillo, A., 2013. Geology, volcanic history and petrology of Vulcano (central Aeolian archipelago), in: Lucchi, F., Peccerillo, A., Keller, J., Tranne, C.A., Rossi, P.L. (Eds.), The Aeolian Islands Volcanoes. Geological Society, London, Memoirs, 37, pp 181-349.

De Astis, G., Peccerillo, A., Kempton, P. D., La Volpe, L., Wu, T.W., 2000. Transition from calc-alkaline to potassium-rich magmatism in subduction environments: geochemical and Sr, Nd, Pb isotopic constraints from the island of Vulcano (Aeolian arc). Contributions to Mineralogy and Petrology 139, 684-03.

Del Moro, A., Gioncada, A., Pinarelli, L., Sbrana, A., Joron, J.L., 1998. Sr, Nd, and Pb isotope evidence for open system evolution at Vulcano, Aeolian Arc, Italy. Lithos 43, 81-106.

Di Traglia, F., Pistolesi, M., Rosi, M., Bonadonna, C., Fusillo, R., Roverato, M., 2013. Growth and erosion: The volcanic geology and morphological evolution of La Fossa (Island of Vulcano, Southern Italy) in the last 1000 years. Geomorphology 194, 94-107. doi:10.1016/j.geomorph.2013.04.018

Finetti, I.R., Del Ben, A., 1986. Geophysical study of the Tyrrhenian opening. Bollettino di Geofisica Teorica e Applicata 28, 75-156.

Francalanci, L., Avanzinelli, R., Tommasini, S., Heuman, A., 2007. A west-east geochemical and isotopic traverse along the volcanism of the Aeolian Island arc, southern Tyrrhenian Sea, Italy: inferences on mantle source processes, in: Beccaluva, L., Bianchini, G., Wilson, M. (Eds.), Cenozoic Volcanism in the Mediterranean Area. Geological Society of America, Denver, U.S.A., pp. 235–263.

Franzini, M., Leoni, L., Saitta, M., 1972. A simple method to evaluate the matrix effect in X-ray fluorescence analysis. X-ray Spectrometry 1, 151–154.

Frezzotti, M.L., Peccerillo, A., Zanon, V., Nikogosian, I., 2004. Silica-rich Melts in Quartz Xenoliths from Vulcano Island and their Bearing on Processes of Crustal Anatexis and Crust-Magma Interaction beneath the Aeolian Arc, Southern Italy. Journal of Petrology 45, 3-26. doi:10.1093/petrology/egg080.

Fusillo, R., Di Traglia, F., Gioncada, A., Pistolesi, M., Wallace, P.J., Rosi, M., 2015. Deciphering post-caldera volcanism: insight into the Vulcanello (Island of Vulcano, Southern Italy) eruptive activity based on geological and petrological constraints. Bulletin of Volcanology 77, 76-99. http://dx.doi.org/10.1007/s00445-015-0963-6.

Gioncada, A., Clocchiatti, R., Sbrana, A., Bottazzi, P., Massare, D., Ottolini, L., 1998. A study of melt inclusions at Vulcano (Aeolian Islands, Italy): insights on the primitive magmas and on the volcanic feeding system. Bulletin of Volcanology 60, 286-306.

Gioncada, A., Mazzuoli, R., Bisson, M., Pareschi, M.T., 2003. Petrology of volcanic products younger than 42 ka on the Lipari-Vulcano Complex (Aeolian Islands, Italy): an example of volcanism controlled by tectonics. Journal of Volcanology and Geothermal Research 122, 191-220.

Granieri, D., Carapezza, M.L., Chiodini, G., Avino, R., Caliro, S., Ranaldi, M., Ricci, T., Tarchini, L., 2006. Correlated increase in CO_2 fumarolic content and diffuse emission from La Fossa crater (Vulcano, Italy): evidence of volcanic unrest or increasing gas release from a stationary deep

magma body? Geophysical Research Letters 33, L13316. http://dx.doi.org/10.1029/2006GL026460.
Harrison, D., Barry, T., Turner, G., 2004. Possible diffusive fractionation of helium isotopes in olivine and clinopyroxene phenocrysts. European Journal of Mineralogy 16, 213-220.
Hilton, D.R., Fischer, T.P., Marty, B., 2002. Noble gases and volatile recycling at subduction zones, in: Porcelli, D.P., Ballentine, C.J., Wieler, R. (Eds.), Noble gases in geochemistry and cosmochemistry. Rev. Mineral. Geochem., 47. Mineral. Soc. of Am, Washington, D.C., pp. 319-370.
Hilton, D.R., Hoogewerff, J.A., Van Bergen, M.J., Hammerschmidt, K., 1992. Mapping magma sources in the east Sunda-Banda arcs, Indonesia: Constraints from helium isotopes. Geochimica et Cosmochimica Acta 56, 851-859.
Hilton, D.R., Macpherson, C.G., Elliott, T.R., 2000. Helium isotope variations in mafic phenocrysts and geothermal fluids from La Palma, The Canary Islands (Spain): implications for HIMU mantle sources. Geochimica et Cosmochimica Acta 64, 2119-2132.
Hoke, L., Lamb, S., Hilton, D.R., Poreda, R.J., 2000. Southern limit of mantle-derived geothermal helium emissions in Tibet: implications for lithospheric structure. Earth and Planetary Science Letters 180, 297-308. http://dx.doi.org/10.1016/S0012-821X(00)00174-6.
Iacono-Marziano, G., Paonita, A., Rizzo, A., Scaillet, B., Gaillard, F., 2010. Noble gas solubilities in silicate melts: New experimental results and a comprehensive model of the effects of liquid composition, temperature and pressure. Chemical Geology 279, 145-157.
Inguaggiato, S., Mazot, A., Diliberto, I.S., Inguaggiato, C., Madonia, P., Rouwet, D., Vita, F., 2012. Total CO_2 output from Vulcano island (Aeolian Islands, Italy). Geochemistry Geophysics Geosystems 13 (2), Q02012. http://dx.doi.org/10.1029/2011GC003920.
Italiano, F. Nuccio, P.M., 1997. Variazione del rapport isotopico $^{3}He/^{4}He$ nelle esalazioni fumaroliche di Vulcano, in: La Volpe, L., Dellino, P., Nuccio, P.M., Privitera, E., Sbrana, A. (Eds.), Progetto Vulcano: Risultati dell'Attività di Ricerca 1993-95. Felici Editore, Pisa, pp. 124-127.
Italiano, F., Pecoraino, G., Nuccio, P.M., 1998. Steam output from fumaroles of an active volcano: tectonic and magmatic hydrothermal controls on the degassing system at Vulcano (Aeolian arc). Journal of Geophysical Research 103, 29829-29842. http://dx.doi.org/10.1029/98JB02237.
Keller, J., 1980. The island of Vulcano. Rendicondi della Società Italiana di Mineralogia e Petrografia 3, 6, 369-414.
Lal, D., 1991. Cosmic ray labeling of erosion surfaces: in situ nuclide production rates and erosion models. Earth Planetary Science Letters 104, 424-439.
Le Maitre, R.W., 2002. Igneous rocks. A classification and glossary of terms, 2nd ed. Recommendations of the IUGS Subcomission on the Systematics of Igneous Rocks. Cambridge University Press, p. 236.
Lippolt, H.J., Weigel, E., 1988. ^{4}He diffusion in ^{40}Ar-retentive minerals. Geochimica et Cosmochimica Acta 52, 1449-1458.
Magro, G., 1997. La composizione isotopica dell'He e dell'Ar nei prodotti di Vulcano: inclusioni fluide e gas fumarolici, in: La Volpe, L., Dellino, P., Nuccio, P.M., Privitera, E., Sbrana, A. (Eds.), Progetto Vulcano: Risultati dell'Attività di Ricerca 1993-95. Felici Editore, Pisa, pp. 124-127.
Martelli, M., Nuccio, P.M., Stuart, F.M., Burgess, R., Ellam, R.M., Italiano, F., 2004. Helium–strontium isotope constraints on mantle evolution beneath the Roman Comagmatic Province, Italy. Earth and Planetary Science Letters 224, 295–308.
Martelli, M., Nuccio, P.M., Stuart, F.M., Di Liberto, V., Ellam, R.M., 2008. Constraints on mantle source and interactions from He-Sr isotope variation in Italian Plio-Quaternary volcanism. Q02001. doi:10.1029/2007GC001730 ISSN: 1525-2027.
Martelli, M., Rizzo, A.L., Renzulli, A., Ridolfi, F., Arienzo, I., Rosciglione, A., 2014. Noble-gas signature of magmas from a heterogeneous mantle wedge: The case of Stromboli volcano (Aeolian Islands, Italy). Chemical Geology 368, 39-53.

884 Marty, B., Trull, T., Luzziez, P., Basile, I., Tanguy, J.C., 1994. He, Ar, O, Sr and Nd isotope
885 constraints on the origin and evolution of Mount Etna magmatism. Earth and Planetary Science
886 Letters 126, 23-39.
887 Mazziotti Tagliani, S., Nicotra, E., Viccaro, M., Gianfagna, A., 2012. Halogen-dominant
888 mineralization at Mt. Calvario dome (Mt. Etna) as a response of volatile flushing into the magma
889 plumbing system. Mineralogy and Petrology 106, 89-105.
890 McDonough, W.F., Sun, S.S., 1995. Composition of the Earth. Chemical Geology 120, 223-253.
891 doi:10.1016/0009-2541(94)00140-4.
892 McKenzie, D., O'Nions, R.K., 1991. Partial melt distributions from inversion of rare Earth element
893 concentrations. Journal of Petrology 32, 1021-1091.
894 Mercalli, G., Silvestri, O., 1891. Le eruzioni dell'isola di Vulcano, incominciate il 3 Agosto 1888 e
895 terminate il 22 Marzo 1890. Ann. Uff. Cent. Meteor. Geodin. I0, 213.
896 Nicotra, E., Viccaro, M., 2012. Transient uprise of gas and gas-rich magma batches fed the
897 pulsating behavior of the 2006 eruptive episodes at Mt. Etna volcano. Journal of Volcanology and
898 Geothermal Research 227-228, 102-118.
899 Nuccio, P.,M., Paonita, A., Sortino, F., 1999. Geochemical modeling of mixing between magmatic
900 and hydrothermal gases: the case of Vulcano, Italy. Earth and Planetary Science Letters 167, 321-
901 333. http://dx.doi.org/10.1016/S0012-821X(99)00037-0.
902 Nuccio, P.M., Paonita, A., 2001. Magmatic degassing of multicomponent vapors and assessment of
903 magma depth: application to Vulcano Island (Italy). Earth and Planetary Science Letters 193, 467-
904 481. http://dx.doi.org/10.1016/S0012-821X(01)00512-X.
905 Nuccio, P.M., Paonita, A., Rizzo, A., Rosciglione, A., 2008. Elemental and isotope covariation of
906 noble gases in mineral phases from Etnean volcanics erupted during 2001-2005, and genetic
907 relation with peripheral gas discharges. Earth and Planetary Science Letters 272, 683-690.
908 Ozima, M., Podosek, F.A., 1983. Noble Gas Geochemistry. Cambridge University Press, pp. 267.
909 Paonita, A., Favara, R., Nuccio, P.M., Sortino, F., 2002. Genesis of fumarolic emissions as inferred
910 by isotope mass balances: CO_2 and water at Vulcano Island, Italy. Geochimica et Cosmochimica
911 Acta 66, 759-772. http://dx.doi.org/10.1016/S0016-7037(01)00814-6.
912 Paonita, A., Federico, C., Bonfanti, P., Capasso, G., Inguaggiato, S., Italiano, F., Madonia, P.,
913 Pecoraino, G., Sortino, F., 2013. The episodic and abrupt geochemical changes at La Fossa
914 fumaroles (Vulcano Island, Italy) and related constraints on the dynamics, structure, and
915 compositions of the magmatic system. Geochimica et Cosmochimica Acta 120, 158-178.
916 Parello, F., Allard, P., D'Alessandro, W., Federico, C., Jean-Baptiste, P., Catani, O., 2000. Isotope
917 geochemistry of Pantelleria volcanic fluids, Sicily Channel Rift: a mantle volatile end-member for
918 volcanism in southern Europe. Earth and Planetary Science Letters 180, 325– 339.
919 Parfitt, E.A., Wilson, L., 2008. Fundamentals of Physical Volcanology. Blackwell Science Ltd,
920 USA, pp. 219.
921 Patterson, D.B., Farley, K.A., McInnes, B.I.A., 1997. Helium isotopic composition of the Tabar-
922 Lihir-Tanga-Feni island arc, Papua New Guinea. Geochimica et Cosmochimica Acta 61, 2485-
923 2496.
924 Peccerillo, A., De Astis, G., Faraone, D., Forni, F., Frezzotti, M.L., 2013. Compositional variation
925 of magmas in the Aeolian arc: implications for petrogenesis and geodymics. Geological Society,
926 London, Memoirs 37, 491-510. doi: 10.1144/M37.15.
927 Peccerillo, A., Frezzotti, M.L., De Astis, G., Ventura, G., 2006. Modeling the magma plumbing
928 system of Vulcano (Aeolian Islands, Italy) by integrated fluid-inclusion geobarometry, petrology,
929 and geophysics. Geology 34, 17-20. http://dx.doi.org/10.0030/G22117.1.
930 Piochi, M., DeAstis, G., Petrelli, M., Ventura, G., Sulpizio, R., Zanetti, A., 2009. Constraining the
931 recent plumbing system of Vulcano (Aeolian Arc, Italy) by textural, petrological, and fractal
932 analysis: The 1739 A.D. Pietre Cotte lava flow. Geochemistry Geophysics Geosystem 10.
933 http://dx.doi.org/10.1029/ 2008GC002176.

Rizzo, A.L., Barberi, F., Carapezza, M.L., Di Piazza, A., Francalanci, L., Sortino, F., D'Alessandro, W., 2015. New mafic magma refilling a quiescent volcano: Evidence from He-Ne-Ar isotopes during the 2011–2012 unrest at Santorini, Greece. Geochemistry, Geophysics, Geosystems 16 (3), 798-814.

Sano, Y., Wakita, H., 1988. Helium isotope ratio and heat discharge rate in the Hokkaido island, Northwest Japan. Geochemistry Journal 22, 293-303.

Sarda, P., Staudacher, T., Allègre, C.J., Lecomte, A., 1993. Cosmogenic neon and helium at Réunion: measurement of erosion rate. Earth and Planetary Science Letters 119, 405-417.

Schiano, P., Clocchiatti, R., Ottolini, L., Sbrana, A., 2004. The relationship between potassic, calc-alkaline and Na-alkaline magmatism in South Italy volcanoes: A melt inclusion approach. Earth and Planetary Science Letters 220, 121-137.

Shaw, A.M., Hilton, D.R., Fisher, T.P., Walker, J.A., De Leeuw, G.A., 2006. Helium isotope variations in mineral separates from Costa Rica and Nicaragua: assessing crustal contributions, timescale variations and diffusion-related mechanisms. Chemical Geology 230, 124-129.

Shimizu, A., Sumino, H., Nagao, K., Notsu, K., Mitropoulos, P., 2005. Variation in noble gas isotopic composition of gas samples from the Aegean arc, Greece. Journal of Volcanology and Geothermal Research 140, 321-339.

Taran, Y., 2011. N_2, Ar, and He as a tool for discriminating sources of volcanic fluids with application to Vulcano, Italy. Bulletin of Volcanology 73, 395-408. http://dx.doi.org/10.1007/s00445-011-0448-1.

Tedesco, D., 1995. Fluid geochemistry at Vulcano Island: a change in volcanic regime or fluctuations in the mixing of different systems? Journal of Geophysical Research 100, 4157-4167. http://dx.doi.org/10.1029/94JB02595.

Tedesco, D., Nagao, K., 1996. Radiogenic ^{4}He, ^{21}Ne and ^{40}Ar in fumarolic gases on Vulcano: implication for the presence of continental crust beneath the island. Earth and Planetary Science Letters 144, 517-528. http://dx.doi.org/10.1016/S0012-821X(96)00196-3.

Tedesco, D., Scarsi, P., 1999. Intensive gas sampling of noble gases and carbon at Vulcano (Southern Italy). Journal of Geophysical Research 104, 10499-10510.

Thirlwall, M.F., 2002. Multicollector ICP-MS analysis of Pb isotopes, using a (207)Pb-(204)Pb double spike, demonstrates up to 400ppm/amu systematic errors in Tl normalization. Chemical Geology 184, 255-279.

Trull, T.W., Kurz, M.D., 1993. Experimental measurements of ^{3}He and ^{4}He mobility in olivine and clinopyroxene at magmatic temperatures. Geochim. Cosmochim. Acta 57, 1313-1324.

Van Soest, M.C., Hilton, D.R., Machperson, C.G., Mattey, D.P., 2002. Resolving sediment subduction and crustal contamination in the Lesser Antilles Island Arc: a combined He-O-Sr isotope approach. Journal of Petrology 43, 143-170.

Ventura, G., 2013. Kinematics of the Aeolian volcanism (Southern Tyrrhenian Sea) from geophysical and geological data, in: Lucchi, F., Peccerillo, A., Keller, J., Tranne, C.A., Rossi, P.L. (Eds.), The Aeolian Islands Volcanoes. Geological Society, London, Memoirs, 37: 3-11. doi: http://dx.doi.org/10.1144/M37.2.

Viccaro M., Nicotra E., Millar I.L., Cristofolini R., 2011. The magma source at Mount Etna volcano: perspectives from the Hf isotope composition of historic and recent lavas. Chemical Geology 281, 343-351.

Zanon, V., Frezzotti, M.L., Peccerillo, A., 2003. Magmatic feeding system and crustal magma accumulation beneath Vulcano Island (Italy): evidence from CO_2 fluid inclusions in quartz xenoliths. Journal of Geophysical Research 108, 2298. http://dx.doi.org/10.1029/2002JB002140.

Fig.1 Simplified geological map of Vulcano Island modified after De Astis et al. (1997), showing the location of the analysed rock samples belonging to different eruptive stages of the Island.

Fig.2 Total Alcali Silica classification diagram (Le Maitre, 2002) for analyzed rock samples. The diamonds represent our data and they are compared with literature data (circles), showing good correspondence. B= basalt, SHO= shoshonite, LT= latite, TR= trachyte, RY= rhyolite.

Fig.3 Variation diagrams for some major and trace elements with silica.

Fig.4 Multi-element diagram normalized to the Primordial Mantle (McDonough and Sun, 1995).

Fig.5 Variation diagrams for Sr and Pb isotopic ratios. All samples trend towards the Calabrian basement composition (Caggianelli et al., 1991; Del Moro et al., 1998) related to crustal assimilation processes. Symbols as in figure 2.

Fig.6 Plot of $^{3}He/^{4}He$ (expressed in Rc/Ra) vs. He abundance in fluid inclusions hosted in mineral samples. Our isotopic data are similar to those of Martelli et al. (2008). The shaded area represents the variation range of $^{3}He/^{4}He$ ratio for the magmatic endmember feeding the fumarolic gases (5.2-6.2 R/Ra; Paonita et al., 2013). Only basalt of SOM and latite of ROV have $^{3}He/^{4}He$ ratio comparable with the fumarolic fluids.

Fig.7 $^{3}He/^{4}He$ ratio versus the age of the rocks (a), their potassium content (b) and Mg# (c). For CG and PGR samples the K_2O wt.% and Mg# data are from Keller (1980), De Astis et al. (1997), Del Moro et al. (1998). Symbols as in Figure 6.

Fig.8 Plot of $^{87}Sr/^{86}Sr$ vs $^{3}He/^{4}He$ plot. The curves show the mixing process between the continental Calabrian crust end-member and pristine magmas directly coming from mantle source (see text). a) mixing of crust with two pristine magmas having different Sr isotopic compositions: the less contaminated one (with lower $^{87}Sr/^{86}Sr$) being related to the rocks older than 30 ka (grey dashed lines), the most enriched one related to the younger rocks (black dashed lines). b) mixing with a single magmatic end-member for all products. For each possible magmatic endmember, modelled mixing curves are shown for three different initial magma He concentrations ($1\cdot10^{-10}$, $2\cdot10^{-10}$, $5\cdot10^{-10}$ mol/g from left to right). In all the cases, ROV shows anomalously high $^{3}He/^{4}He$ values. An input of deep magmatic gases in latitic reservoir could increase the $^{3}He/^{4}He$ ratio in magmatic body without change Sr isotopic ratio (arrow in a and b). c) The plot shows the best fitting curve for all analyzed products between the magmatic end-member and Calabrian crust.

1021

Not provided.

Figure1

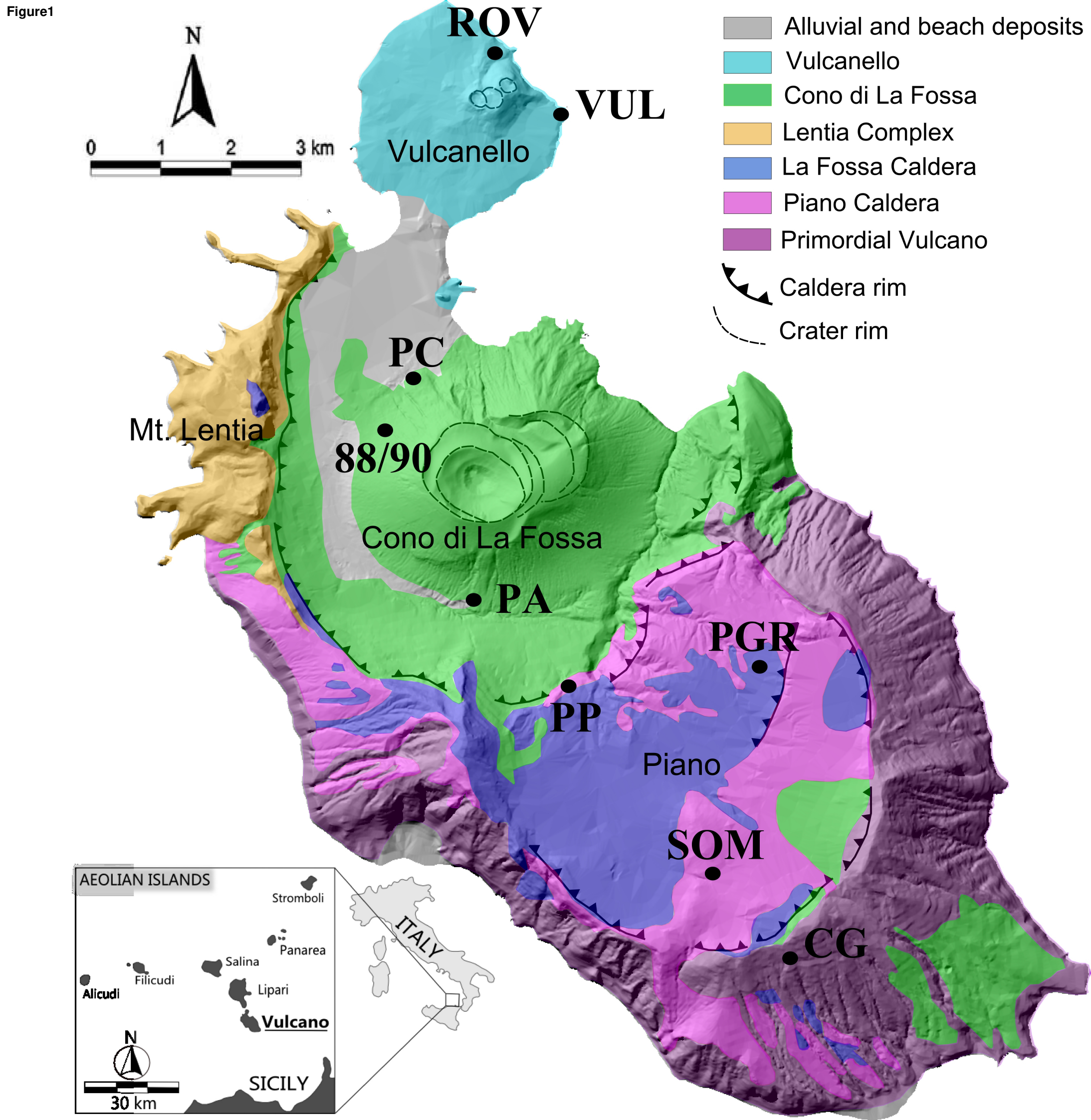
N
0
1
2
3 km
ROV
VUL
Vulcanello
PC
Mt. Lentia
88/90
Cono di La Fossa
PA
PGR
PP
Piano
SOM
CG
Alluvial and beach deposits
Vulcanello
Cono di La Fossa
Lentia Complex
La Fossa Caldera
Piano Caldera
Primordial Vulcano
Caldera rim
Crater rim
AEOLIAN ISLANDS
Stromboli
Panarea
Salina
Filicudi
Alicudi
Lipari
Vulcano
N
30 km
SICILY
ITALY

Figure2

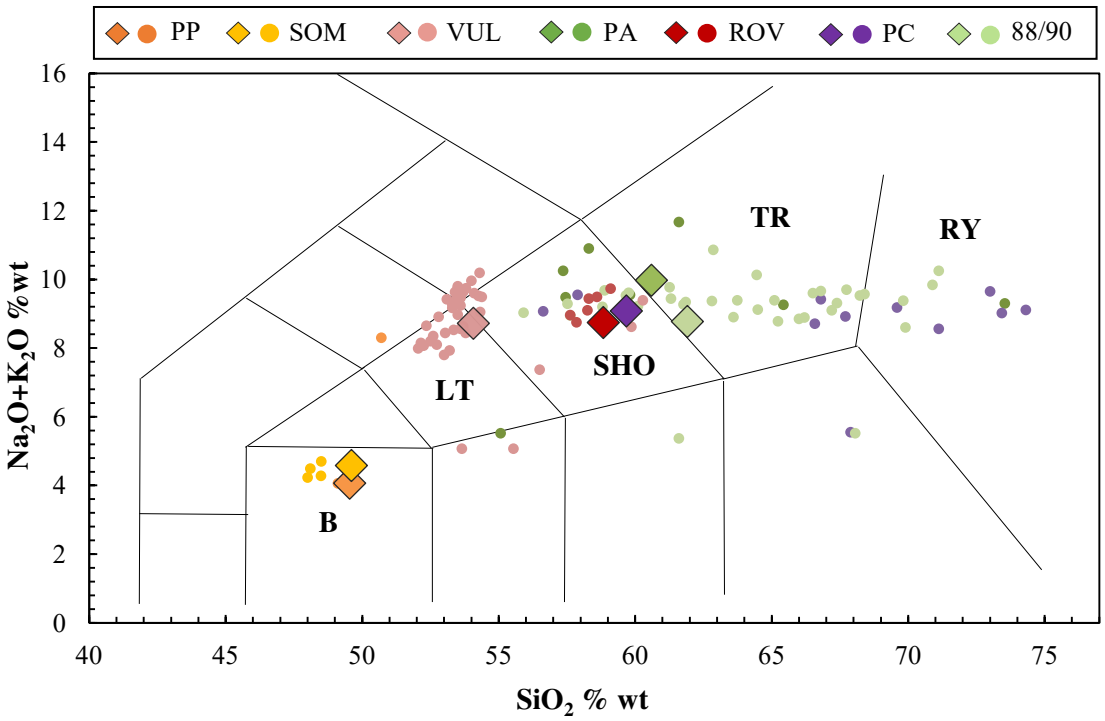
PP
SOM
VUL
PA
ROV
PC
88/90
TR
RY
SHO
LT
B
Na2O+K2O %wt
SiO2 % wt
0
2
4
6
8
10
12
14
16
40
45
50
55
60
65
70
75

Figure3

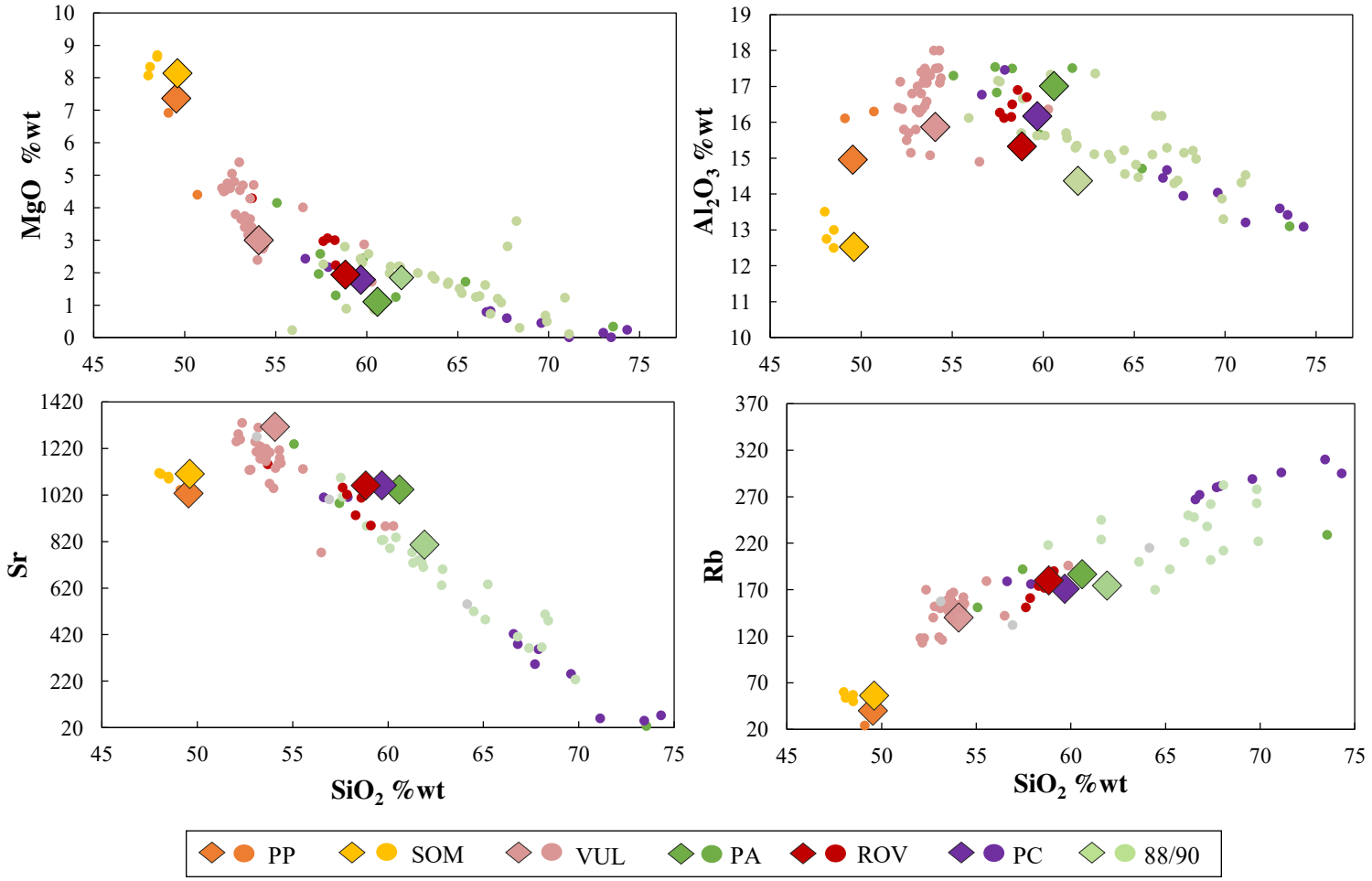

Figure4

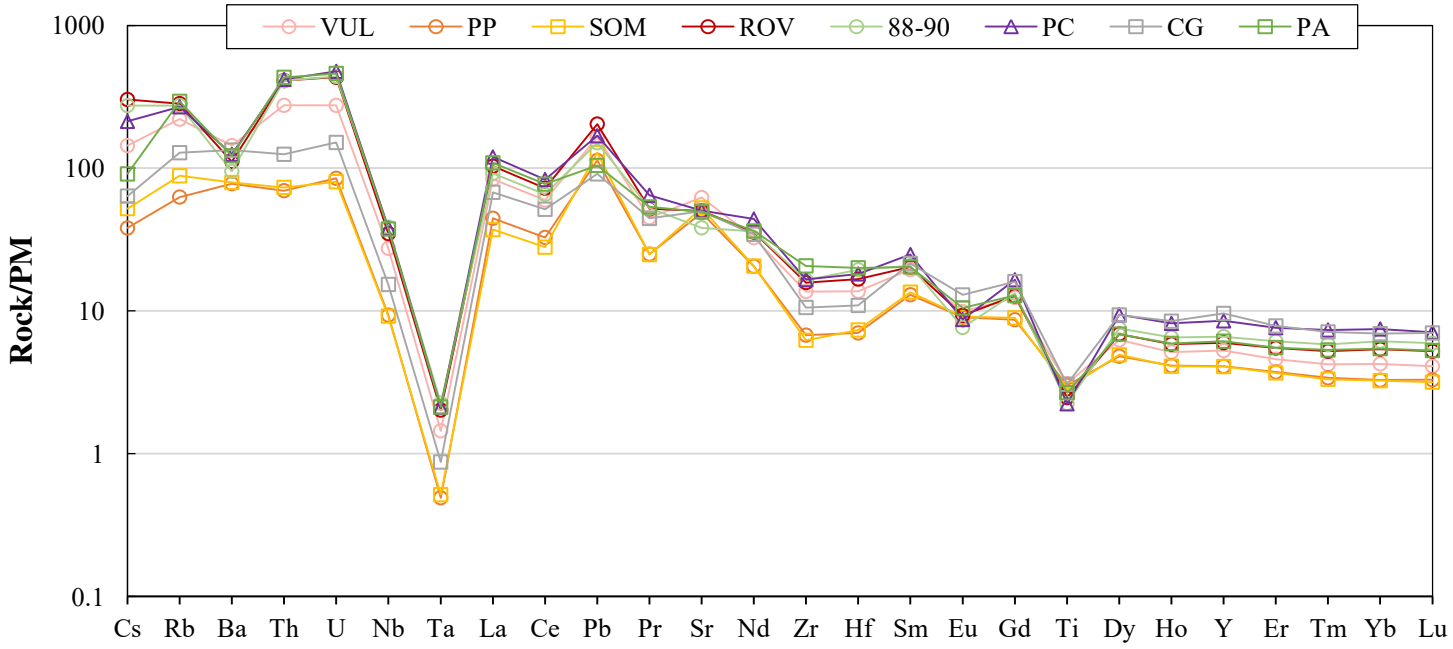
VUL
PP
SOM
ROV
88-90
PC
CG
PA
1000
100
10
1
0.1
Rock/PM
Cs
Rb
Ba
Th
U
Nb
Ta
La
Ce
Pb
Pr
Sr
Nd
Zr
Hf
Sm
Eu
Gd
Ti
Dy
Ho
Y
Er
Tm
Yb
Lu

Figure5

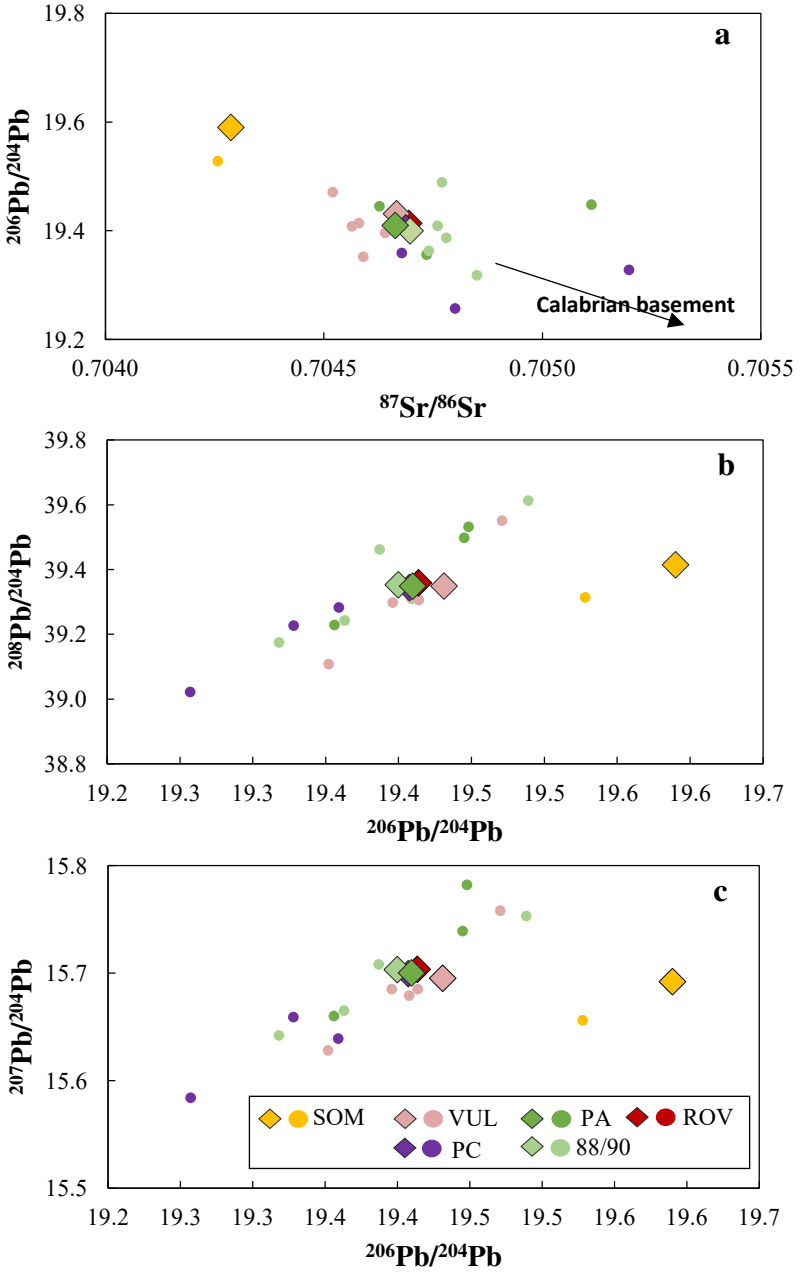
a
19.8
19.6
19.4
19.2
$^{206}Pb/^{204}Pb$
0.7040
0.7045
0.7050
0.7055
$^{87}Sr/^{86}Sr$
Calabrian basement
b
39.8
39.6
39.4
39.2
39.0
38.8
$^{208}Pb/^{204}Pb$
19.2
19.3
19.3
19.4
19.4
19.5
19.5
19.6
19.6
19.7
$^{206}Pb/^{204}Pb$
c
15.8
15.7
15.6
15.5
$^{207}Pb/^{204}Pb$
SOM
VUL
PA
ROV
PC
88/90
19.2
19.3
19.3
19.4
19.4
19.5
19.5
19.6
19.6
19.7
$^{206}Pb/^{204}Pb$

Figure6

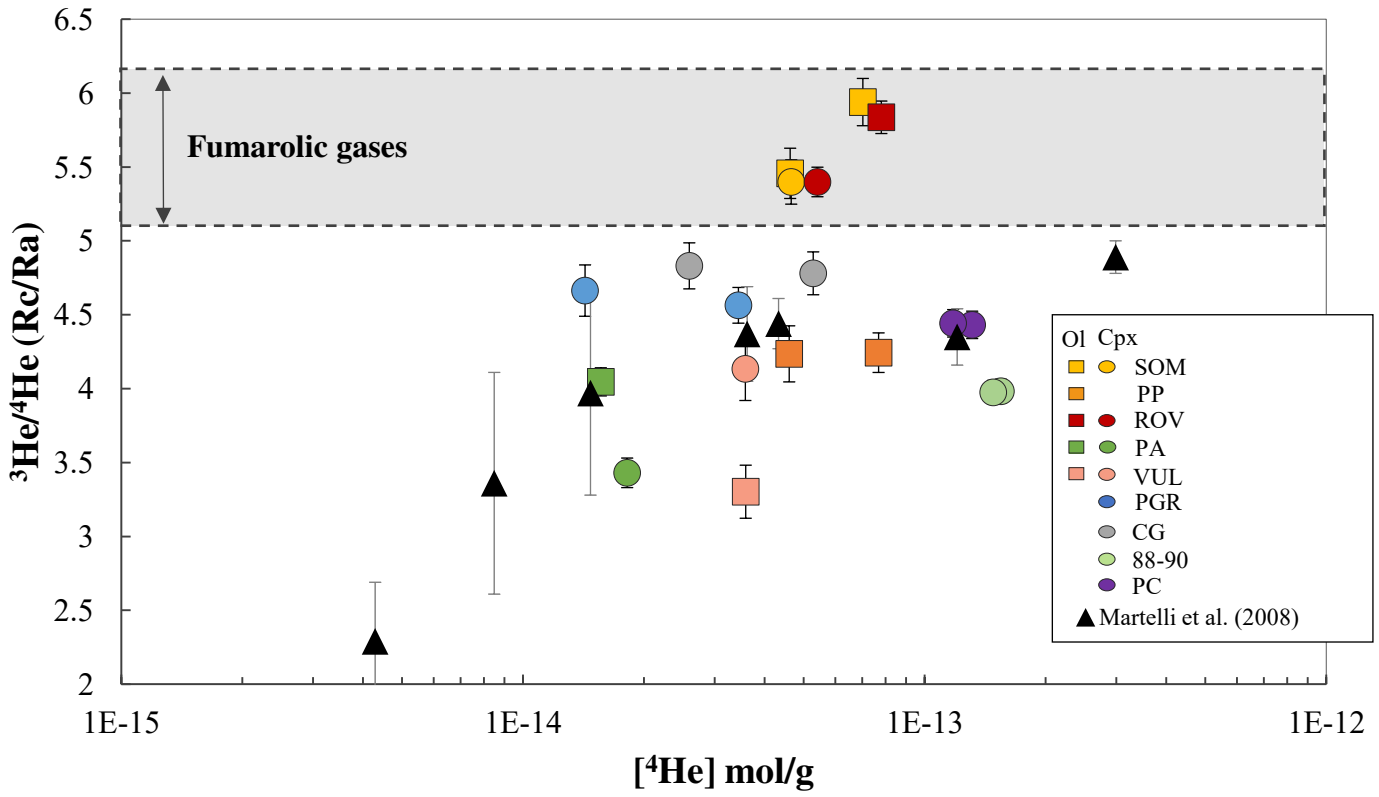
6.5
6
5.5
5
4.5
4
3.5
3
2.5
2
Fumarolic gases
$^3He/^4He$ (Rc/Ra)
1E-15
1E-14
1E-13
1E-12
[^{4}He] mol/g
Ol Cpx
SOM
PP
ROV
PA
VUL
PGR
CG
88-90
PC
Martelli et al. (2008)

Figure7

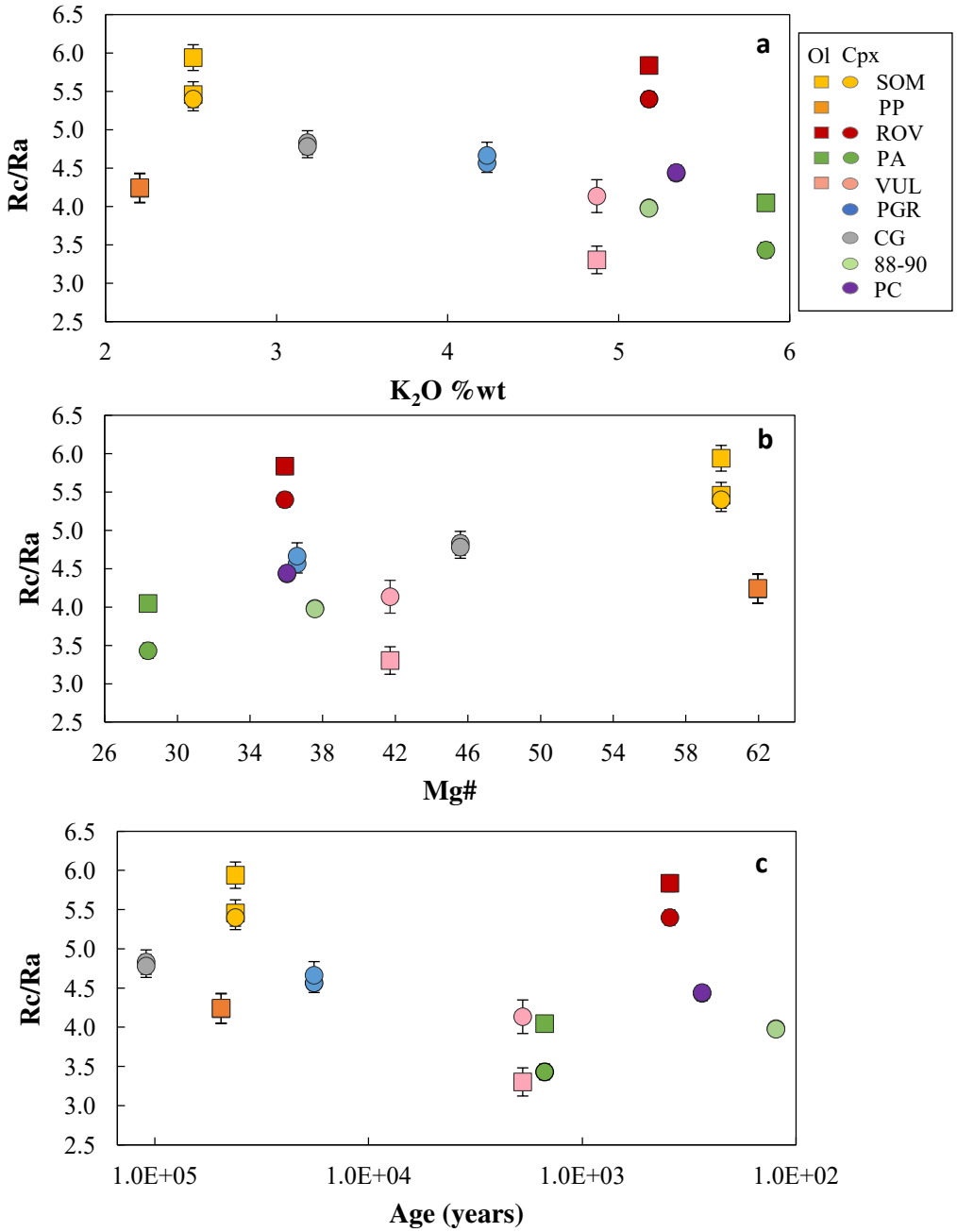
a
Rc/Ra
6.5
6.0
5.5
5.0
4.5
4.0
3.5
3.0
2.5
2
3
4
5
6
K2O %wt
Ol Cpx
SOM
PP
ROV
PA
VUL
PGR
CG
88-90
PC
b
Rc/Ra
26
30
34
38
42
46
50
54
58
62
Mg#
c
Rc/Ra
1.0E+05
1.0E+04
1.0E+03
1.0E+02
Age (years)

Figure8

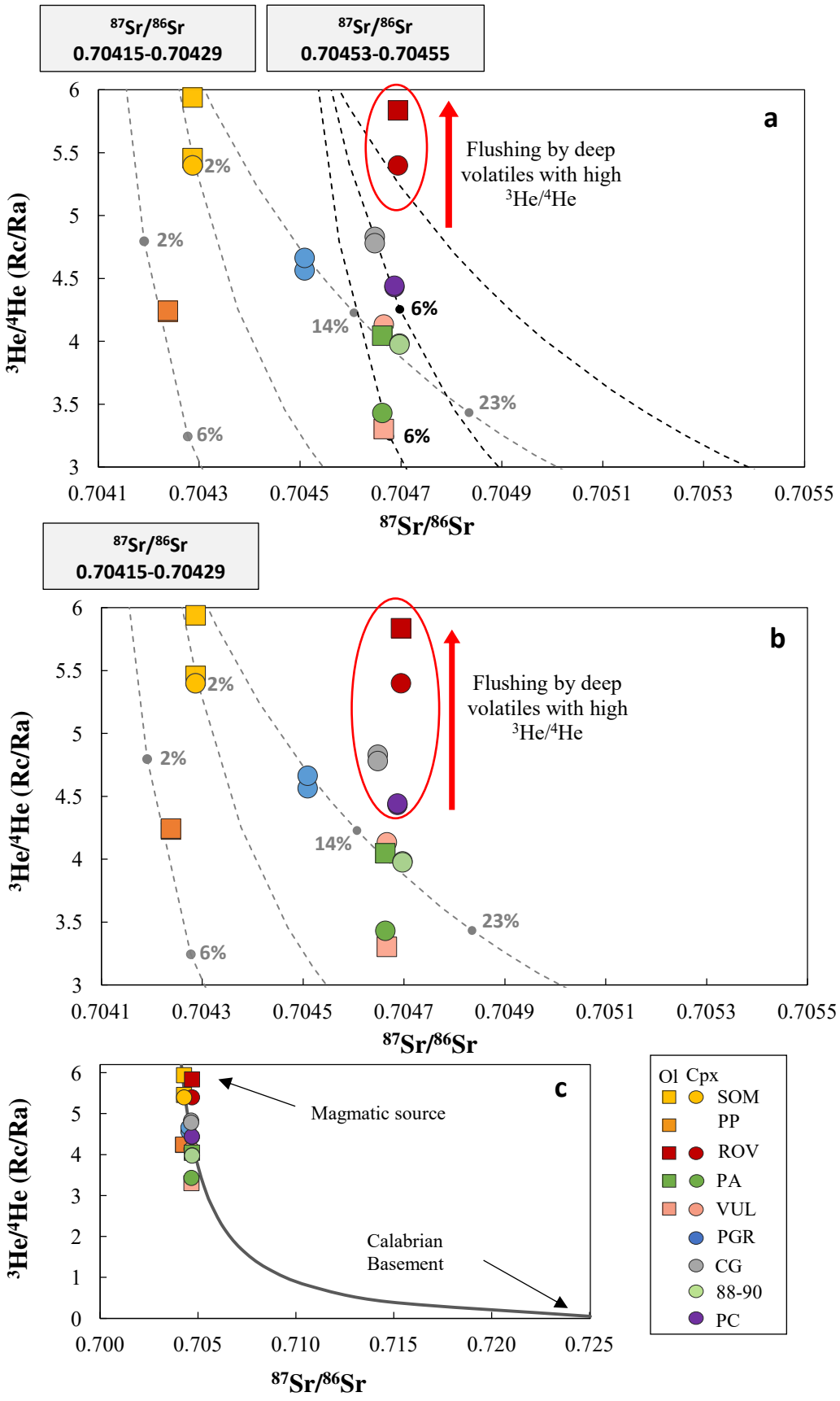
87Sr/86Sr
0.70415-0.70429
87Sr/86Sr
0.70453-0.70455
a
Flushing by deep volatiles with high 3He/4He
2%
2%
6%
14%
23%
6%
6%
3He/4He (Rc/Ra)
87Sr/86Sr
b
c
Magmatic source
Calabrian Basement
Ol Cpx
SOM
PP
ROV
PA
VUL
PGR
CG
88-90
PC

Table1
Click here to download Table: Tab.1.doc

Table 1 Petrographic features of the rock samples.

Sample	**PP**	**SOM**	**PA**	**PC**	**VUL**	**ROV**	**VL315-7**	**VL14-1**
Volcanic system	***La Fossa***	***La Fossa***	***La Fossa***	***La Fossa***	***Vulcanello***	***Vulcanello***	***La Fossa***	***La Fossa***
I.P.(VOL%)	5	3	20	30	25	30	10	5
Groundmass texture	*intersertal micro- to cryptocrystalline*	*hyalopilitic*	*cryptocrystalline*	*hyalopilitic*	*intersertal micro- to cryptocrystalline*	*cryptocrystalline*	*vitrous*	*hyalopilitic*
Cpx (vol%)	70	85	40	45	75	65	60	55
habitus	*euhedral to subhedral*	*euhedral*	*subhedral to euhedral*	*euhedral to subhedral*	*euhedral to subhedral*	*euhedral to subhedral*	*euhedral*	*euhedral*
dimensions	*1-4 mm*	*up to 1 mm*	*up to 3 mm*	*up to 5 mm*	*up to 1.5 mm*	*up to 5 mm*	*up to 2mm*	*up to 1.5 mm*
Pl (vol%)	absent	10	55	40	15	15	30	45
habitus	-	*euhedral*	*euhedral to subhedral*	*euhedral to subhedral*	*subhedral*	*euhedral to subhedral*	*euhedral*	*subhedral to anhedral*
dimensions	-	*500-1200 µm*	*up to 4 mm*	*up to 6 mm*	*up to 1.5 mm*	*up to 5 mm*	*up to 1.5 mm*	*up to 1.5 mm*
Ol (vol%)	30	10	2	absent	5	10	10	absent
habitus	*euhedral to subhedral*	*euhedral*	*anhedral*		*euhedral*	*euhedral*	*subhedral*	-
dimensions	*up to 2 mm*	*up to 700 µm*	*up to 500 µm*		*up to 1.5 mm*	*up to 700 µm*	*300-800 µm*	-
Ox (vol%)	0	absent	5	5	5	5	5	absent
habitus	-	-	*euhedral*	*euhedral*	*euhedral*	*euhedral*	*euhedral*	-
dimensions	-	-	*up to 500 µm*	*up to 400 µm*	*up to 400 µm*	*up to 500 µm*	*up to 500 µm*	-
Glomerophire	absent	absent	yes	yes	absent	absent	absent	yes

Table2
Click here to download Table: Tab.2.docx

Table 2
Major and trace element of whole rock composition for the analysed samples.

	CG	PP	SOM	PA	PC	88-90	VUL	ROV
SiO_2 wt%	n.d.	49.54	49.60	60.60	59.68	61.91	54.07	58.83
TiO_2	n.d.	0.69	0.85	0.48	0.53	0.48	0.72	0.57
Al_2O_3	n.d.	14.96	12.53	17.01	16.17	14.37	15.87	15.33
Fe_2O_3 TOT	n.d.	8.06	9.69	4.96	5.64	5.47	7.47	6.16
MnO	n.d.	0.21	0.23	0.12	0.13	0.14	0.17	0.14
MgO	n.d.	7.37	8.14	1.1	1.78	1.85	3	1.94
CaO	n.d.	11.95	13.67	5.24	6.25	5.85	9.22	6.84
Na_2O	n.d.	1.87	2.07	4.11	3.74	3.6	3.85	3.57
K_2O	n.d.	2.2	2.51	5.86	5.34	5.18	4.87	5.18
P_2O_5	n.d.	0.31	0.24	0.33	0.39	0.25	0.43	0.35
LOI		2.85	0.46	0.19	0.34	0.91	0.33	1.09
Total		100.01	99.99	99.99	99.99	100.01	100.00	100.00
Mg#		61.96	59.95	28.38	36.03	37.57	41.71	35.12
Li	19.37	115.54	11.37	47.42	34.56	44.64	27.93	32.98
Rb	81.52	39.89	56.16	186.67	171.01	174.47	140.09	179.99
Sr	1056	1027	1111	1044	1062	807	1313	1061
Y	42.70	18.62	18.54	27.95	38.79	30.07	23.98	27.25
Zr	118	76	70	232	186	184	153	117
Nb	10.93	6.66	6.56	26.75	27.16	27.54	19.57	24.84
Cs	2.04	1.22	1.67	2.92	6.81	8.79	6.18	9.69
Ba	937	545	555	855	875	664	1006	779
La	46.58	30.62	25.5	74.89	82.33	63.16	57.55	70.95
Ce	91.49	58.11	49.67	137.38	147.88	116.23	106.2	128.75
Pr	12.28	6.90	6.85	14.78	17.84	14.49	12.44	14.35
Nd	46.58	27.84	27.93	49.21	59.63	48.87	44.19	48.33
Sm	9.55	5.77	6.01	9.03	11.03	9.23	8.64	9.03
Eu	2.17	1.51	1.53	1.76	1.46	1.29	1.66	1.56
Gd	9.57	5.18	5.33	7.64	9.86	7.93	7.40	7.60
Tb	1.20	0.68	0.64	1.10	1.25	1.00	0.94	0.99
Dy	6.91	3.55	3.63	5.07	6.92	5.56	4.62	5.08
Ho	1.39	0.68	0.67	0.97	1.34	1.07	0.84	0.96
Er	3.77	1.79	1.77	2.66	3.67	2.95	2.21	2.64
Tm	0.53	0.25	0.25	0.39	0.54	0.43	0.31	0.39
Yb	3.42	1.62	1.60	2.69	3.69	3.03	2.10	2.66
Lu	0.52	0.24	0.23	0.39	0.53	0.44	0.30	0.39
Hf	3.38	2.17	2.27	6.20	5.62	6.01	4.24	5.17
Ta	0.62	0.35	0.37	1.51	1.51	1.61	1.03	1.44
Pb	16.88	20.98	23.73	19.36	31.24	27.91	30.39	37.71
Th	10.64	5.92	6.23	36.82	35.61	34.81	23.43	34.98
U	3.18	1.78	1.69	9.68	10.02	9.24	5.79	9.10

Mg# = 100 × Mg/(Mg + Fe_{tot}); LOI = loss on ignition.

Table3
Click here to download Table: Tab.3.docx

Table 3
Sr and Pb isotopic ratios

Sample	$^{87}Sr/^{86}Sr$	±1σ	$^{206}Pb/^{204}Pb$	±1σ	$^{207}Pb/^{204}Pb$	±1σ	$^{208}Pb/^{204}Pb$	±1σ
SOM	0.704287	0.000006	19.590	0.0010	15.692	0.0005	39.415	0.0016
ROV	0.704694	0.000009	19.414	0.0010	15.703	0.0006	39.359	0.0018
VUL	0.704666	0.000012	19.431	0.0010	15.695	0.0007	39.349	0.0019
PC	0.704687	0.000010	19.407	0.0010	15.699	0.0006	39.345	0.0018
88/90	0.704697	0.000005	19.400	0.0009	15.703	0.0005	39.353	0.0016
PA	0.704663	0.000005	19.410	0.0010	15.700	0.0007	39.349	0.0018

Table4

Click here to download Table: Tab.4.docx

Table 4

Elementary and isotopic composition of noble gases entrapped in fluid inclusions hosted in olivine (Ol), diopside (Di) and augitie (Au) pyroxene.

Sample	Mineral	Weight g	[He] 10^{-14} (mol/g)	[Ne] 10^{-15} (mol/g)	[Ar] 10^{-13} (mol/g)	$^{3}He/^{4}He$ (R/Ra)	$^{3}He/^{4}Hec$ (Rc/Ra)	$Err^{+}/-$	$^{40}Ar/^{36}Ar$	$Err^{+}/-$	$^{4}He/^{20}Ne$
CG	Au	2.0	2.6	0.95	2.9	4.78	4.83	0.080	306.5	0.16	27.4
	Au	2.0	5.3	0.9	6.5	4.76	4.78	0.140	300.9	0.21	58.8
PP	Ol	1.1	4.6	0.71	5.8	4.22	4.24	0.190	304.5	0.5	64.7
	Ol	0.9	7.7	0.7	4.5	4.23	4.24	0.134	319.9	0.6	110.3
	Ol	0.7	0.73	0.71	4.5	-	-		302.5	0.9	10.2
	Di	2.0	0.41	4.4	2.1	-	-		307.5	1.0	0.9
	Di	1.8	0.27	8.0	8.8	-	-		300.0	0.5	0.3
	Di	4.0	0.23	2.2	14.0	-	-		298.7	0.2	1.0
	Au	2.0	0.14	3.4	2.4	-	-		315.7	1.1	0.4
SOM	Ol	1.2	4.6	1.7	2.1	5.40	5.46	0.170	293.5	0.4	27.1
	Ol	1.2	7.0	4.7	2.5	5.83	5.94	0.160	299.2	0.5	14.9
	Di	1.2	4.7	2.4	2.2	5.32	5.40	0.150	302.2	0.7	19.4
PGR	Au	2.0	2.8	0.36	2.0	-	-		312.5	1.3	79.3
	Au	4.1	3.4	0.29	2.8	4.55	4.56	0.121	310.6	0.4	119.3
	Au	4.1	1.4	0.41	2.7	4.63	4.66	0.173	300.0	0.4	34.5
PA	Ol	1.0	1.6	3.3	7.0	3.82	4.05	0.095	306.0	0.4	4.7
	Au	2.1	1.8	9.4	44.0	2.99	3.43	0.100	301.6	0.1	1.9
	Au	4.1	0.77	11	29.0	-	-		303.4	0.1	0.7
PC	Au	1.5	13.0	5.1	8.4	4.39	4.43	0.090	316.0	0.2	25.9
	Au	1.5	12.0	5.5	9.0	4.39	4.44	0.090	314.6	0.3	21.2
88-90	Au	2.0	15.0	4.7	9.7	3.95	3.98	0.080	306.1	0.2	32.8
	Au	2.0	15.0	4.2	9.4	3.95	3.97	0.080	306.5	0.2	35.0
VUL	Ol	1.1	1.9	1.9	6.9	-	-		304.2	0.4	10.1
	Ol	2.0	3.6	3.9	15.0	3.21	3.30	0.180	304.4	0.2	9.3
	Au	2.0	2.8	0.68	2.4	-	-		326.6	1.2	40.7
	Au	2.0	3.0	1.0	2.2	-	-		342.3	1.4	29.5
	Au	4.0	3.6	9.0	39.0	3.86	4.13	0.214	303.8	0.1	4.0
ROV	Ol	1.3	7.8	0.47	4.6	5.83	5.84	0.110	302.5	0.2	165.7
	Au	4.1	5.4	6.2	38.0	5.23	5.40	0.100	297.2	0.1	8.7
AIR						1.00			295.5		0.318

Supplementary Table 1S

Click here to download Background dataset for online publication only: Supplementary_Table_1S.xlsx

Supplementary Table 2S

Click here to download Background dataset for online publication only: Supplementary_Table_2S.xls